University of Stuttgart
Germany

IFB
Institut für Flugzeugbau
Institute of Aircraft Design

Conceptual Design and Analysis of a High-Efficient Low-Emission Supersonic Aircraft HELESA

Joint NASA / DLR Aeronautics Design Challenge 2016-2017

Institute of Aircraft Design
University Stuttgart

Daniel Silberhorn
Dominik Schaupp

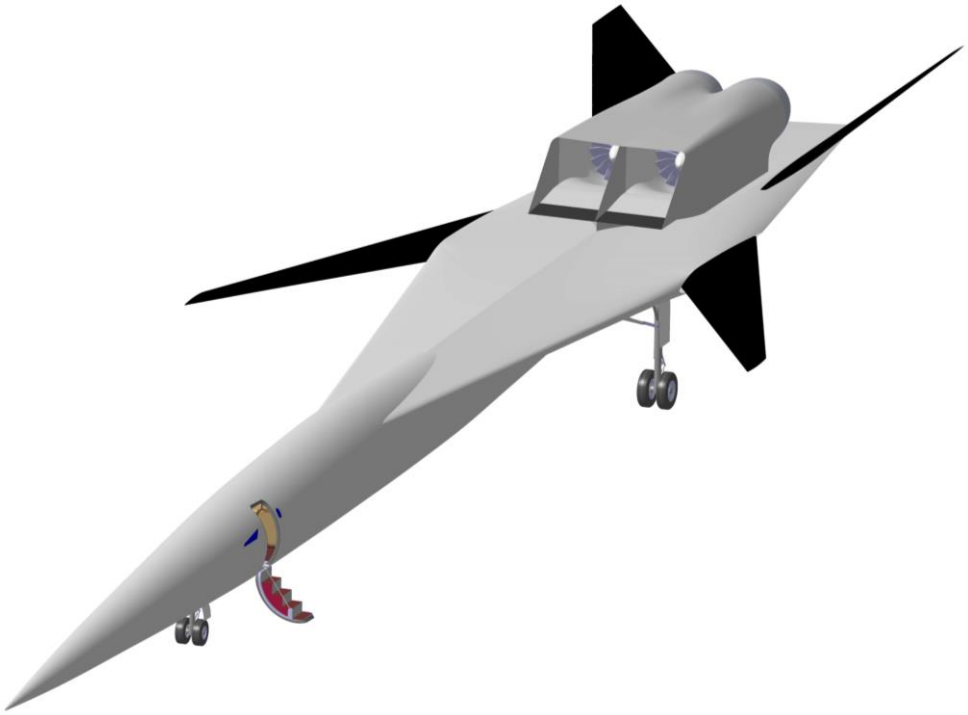

Faculty Tutor: M.Sc. Marco Rizzato

07/01/2017

Members of the student team

Schaupp	Dominik	5th Semester in Master Programme
Silberhorn	Daniel	4th Semester in Master Programme

Abstract

The end of the Concorde in 2003 meant also the end of commercial supersonic transport until today. However, various companies and start-ups such as Aerion Corporation and Boom Technology as well as research institutions such as NASA still believe in the concept of commercial supersonic transport and, in the last years, have been developing aircraft and technologies to try to make it technically and economically feasible. In order for commercial supersonic transport to be viable, the research focus must lie on the minimization of its environmental impact through a drastic increase in fuel efficiency, a substantial decrease in pollutant emissions as well as a reduction in generated noise, both in the vicinity of airports and at supersonic speeds. As part of the Joint NASA/DLR Aeronautics Design Challenge 2016/17 a conceptual aircraft design with entry-into-service in 2025 that can meet such stringent criteria is to be proposed by a student team. The task has been addressed in an interdisciplinary way, starting with a thorough analysis of the state of the art and the available technology while considering the economics of the possible missions. Then a study of the appropriate aircraft configuration in terms of fuselage, cabin and wing design has been carried out, before moving on to a thorough aerodynamic design and analysis. Eventually the performance of the aircraft and its comparison with appropriate reference aircraft is presented. The whole design has been based on standard literature on aircraft design and supersonic flight as well as on numerous scientific papers, Ph.D. theses and publications. The result of this study is HELESA – High-Efficient Low-Emission Supersonic Aircraft – an aircraft which meets and partially even exceeds the prescribed design goals.

Universität Stuttgart

Institut für Flugzeugbau - Bereich Flugzeugentwurf
Prof. Dr.-Ing.
Andreas Strohmayer

Kontakt
Pfaffenwaldring 31
70569 Stuttgart
T 0711 685-69567
F 0711 685-62449
E-Mail:
strohmayer@ifb.uni-stuttgart.de
www.ifb.uni-stuttgart.de

Universität Stuttgart
Institut für Flugzeugbau • Pfaffenwaldring 31 • 70569 Stuttgart

The hereby submitted report "High-Efficiency Low-Emission Supersonic Aircraft – HELESA" is the work of Master students Daniel Silberhorn and Dominik Schaupp, currently enrolled at the University of Stuttgart. It has been examined and is endorsed by the Institute of Aircraft Design for the participation in the Joint NASA/DLR Aeronautics Design Challenge 2016-17.

M.Sc. Marco Rizzato

Content

1 Introduction 1
2 The Configuration 2
3 Design Process 3
4 The HELESA Design 4
4.1 Cabin Design 4
4.2 Aerodynamics 5
4.2.1 Subsonic Regime 5
4.2.2 Transonic Regime 6
4.2.3 Supersonic Regime 6
4.2.4 The Wing 9
4.2.5 Canard versus V-Tail 12
4.2.6 Aerodynamic Efficiency versus Structural Mass 12
4.2.7 Wave Rider 13
4.3 Mass Prediction and Stability 13
4.3.1 Mass Prediction 13
4.3.2 Stability 15
4.4 Propulsion 15
4.4.1 The Engine 15
4.4.2 The Intake 17
4.4.3 Nitrogen Oxide Emissions 17
4.5 Systems 18
4.5.1 High-Lift 18
4.5.2 Landing Gear 19
4.5.3 Battery 19
4.5.4 Electric Ground Taxi System 19
4.5.5 Flight Controls 20
4.6 Noise 20
4.6.1 ICAO Noise Regulations 20
4.6.2 Sonic Boom 21
4.7 The Mission 22
4.7.1 Possible Missions 22
4.7.2 Maximum Cruise Altitude 22
4.7.3 Ground Operation 22
4.8 Concluding Studies 23
5 Conclusion 24
6 Acknowledgment 24
List of References 25
Appendix 32

1 Introduction

This report is about the conceptual design of a commercial supersonic airplane for 2025. The main goals to be achieved are:

- → Cruise Mach number of 1.6 – 1.8
- → Design range of 4,000nm
- → Payload of 6 to 20 passenger
- → Fuel efficiency of at least 3.55 passenger-kilometer per kilograms of fuel.
- → Take-off field length less than 2,133m

Further aims, defined by NASA, for the next generation of business-jets are a sonic boom between 70-75PLdB, airport noise according to ICAO chapter 14 and cruise NOx emissions comparable to current transonic aircraft. How to cope with these requirements is content of this study.

Challenge of supersonic flight

By breaking the sound barrier, characteristics arise which are not known from subsonic flight. To name some aspects we first have a brief look on fuel efficiency by consulting the well-known Breguet equation (1-1).

$$R = \frac{v}{c_{TL}} \cdot \frac{L}{D} \cdot ln\left(\frac{m_{start}}{m_{landing}}\right) \qquad (1\text{-}1)$$

It can be seen, that three parameters are improvable to achieve an efficient design: Low-drag aerodynamics or high lift-to-drag ratio (L/D), lightweight structure and low specific fuel consumption c_{TL}.

Efficient supersonic aerodynamics is achieved for instance through a slender fuselage as well as thin wings. Unfortunately, such design would result in a structural weight penalty.

Furthermore, an additional drag form occurs caused by the formation of shockwaves called wave drag. This makes it challenging to get at least near the efficiency, subsonic airplanes achieve. Finally, the propulsion efficiency in terms of the thrust specific fuel consumption c_{TL} is considered. Because of the low bypass ratio, caused by the need of a slender engine with a high specific thrust and a high exhaust speed, achieving high efficiency as well as low noise at take-off is again demanding.

Another challenge is the sonic boom. Without special consideration, the ambitious aim of 75dB perceived noise level cannot be satisfied for business class airplanes. However, almost all design aspects required to mitigate the sonic boom are in contradiction to the fuel efficiency and low emission ambition. [1]

Nevertheless, the potential of supersonic business aircraft lies in the opportunity of substantial time saving. Looking at a mission between London and New York, a one day trip becomes possible. Starting at 9:00 a.m. in London and arriving at 8:00 a.m. local time in New York, the flight back takes off at 02:00 p.m. to be back in London at 11:00 p.m.. [2]

Summarizing, there are a lot of challenges to cope with and compromises must be made to achieve an efficient and economical successful aircraft. Having this in mind, the design is orientated towards fuel efficiency and environmental sensibility, neglecting the low-boom design aspect which results in the observation of the current regulations concerning supersonic flight over land.

The underlying literature ranges from primary sources if profound methods and fundamentals were discussed to contemporary literature if assumptions concerning new technologies are made.

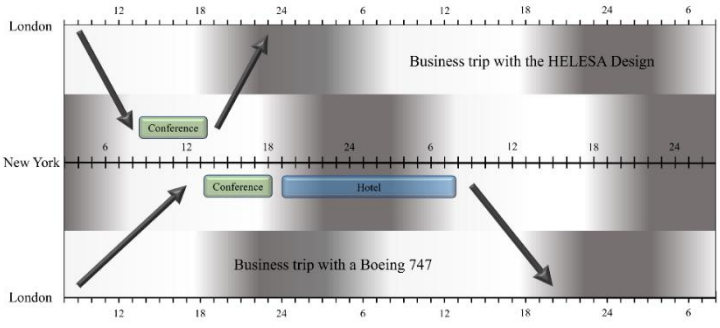

Figure 1. Time saving potential [6]

2 The Configuration

In this section, a short, general description of the main features and characteristics of the High-Efficient Low-Emission Supersonic Aircraft (HELESA) is provided. The configuration determination is described in detail throughout the report.

An airplane for 18 passengers with a long slender fuselage having almost no windows has built the basis of the design. The rear part of the fuselage is merged into a wing with a sweep angle of 80°, comparable with a strake. At the tip of this inner wing, a variable forward swept wing is mounted which can be turned from 20° to 58°, measured positive forward. The airplane is inspired by the More Electric Aircraft (MEA) [3] concept. Instead of an auxiliary power unit (APU) there is a battery in the fuselage tip, followed by the baggage compartment, the air-conditioning and the nose landing gear. After the pressure bulkhead, a synthetic vision cockpit is applied with windows on each side followed by the passenger cabin with the lavatory at its end. The fuel is stored in the rear part of the fuselage as well as in the inner and outer wing. On top of the inner wing, two engines are attached with a takeoff thrust of 95kN each and a bypass ratio of 2.5, followed by a V-tail.

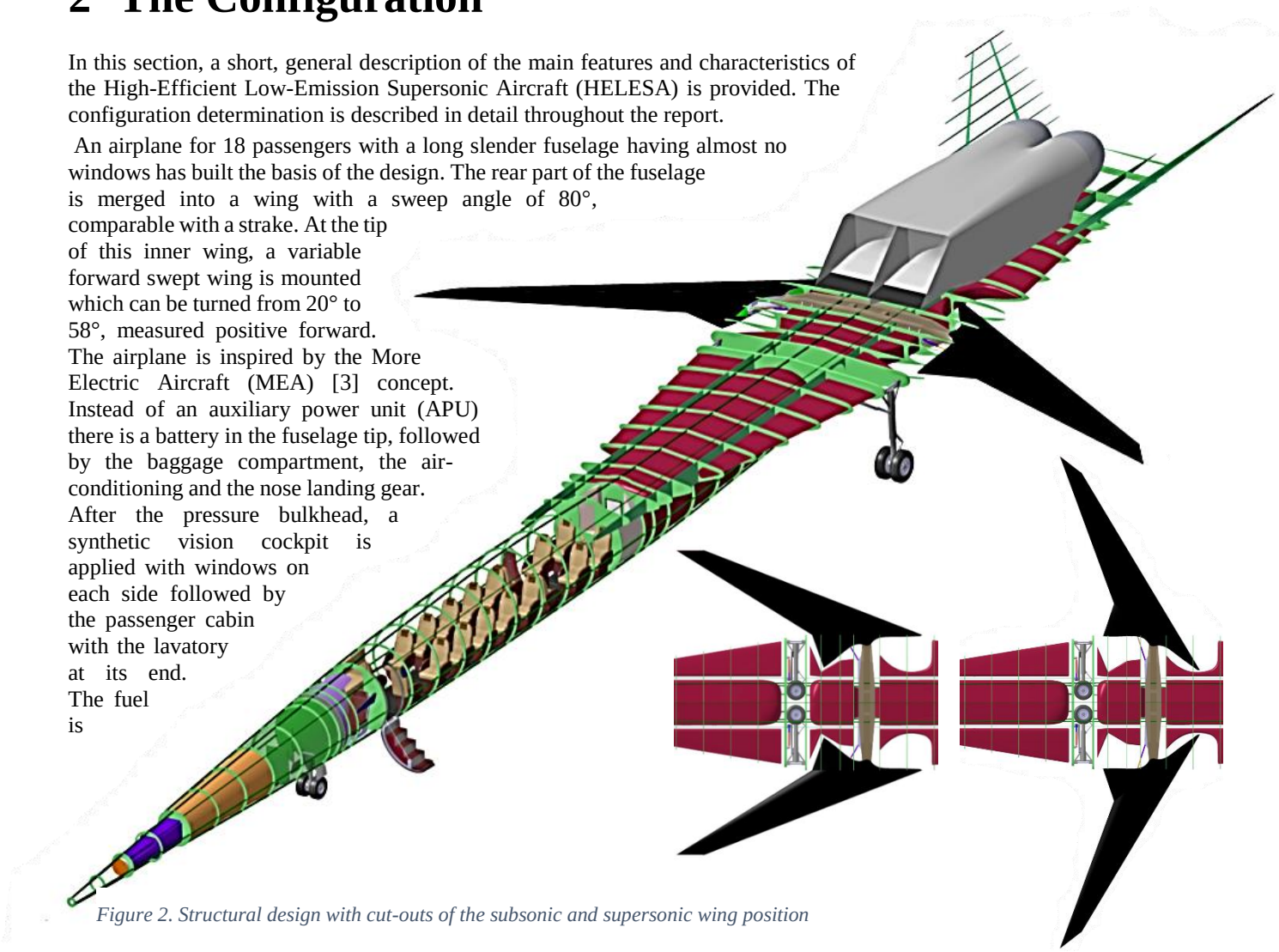

Figure 2. Structural design with cut-outs of the subsonic and supersonic wing position

The structural configuration and relevant data are shown in Figure 2 and Table 1.

Crew	2
Capacity	18 passengers
Length	41m
Wingspan (take-off/landing)	18.3m
Wingspan (subsonic cruise)	14.1m
Wingspan (supersonic cruise)	11.2m
Wing area	98m^2
Design payload	1,890kg
Max take-off mass	43,100kg
Operating mass empty	19,577kg
Maximum lift coefficient	1.75

Cruise Mach number supersonic	1.6
Cruise Mach number transonic	0.92
Range supersonic cruise	4,000nm
Range subsonic cruise	4,750nm
Service ceiling	17km
Take-off field length (SL, ISA, MTOM)	1,900m
Landing distance (SL, ISA, MLW)	1,150m
Thrust loading	0.45
Wing loading	445kg/m^2
Take-off thrust	189.5kN
Fuel efficiency	6.6 pkm/kg

Table 1. General HELESA data

3 Design Process

In this section, the schematic design procedure, shown in Figure 3, is described. The requirements are setting the starting point, followed by the mission definition and the computation of the design diagram shown in Figure 4, which is inspired by Strohmayer [4]. The axis of ordinate of this diagram describes the thrust loading and the axis of abscissae the wing loading of the aircraft. With an estimated value of MTOM from the mission calculation, the result of this diagram provides the reference wing area as well as the maximum take-off thrust. The goal in terms of fuel efficiency is to realize a design with a low thrust loading for smaller and lighter engines and a high wing loading for reduced wetted area. So, the red dot, representing the design point, should be placed near the right bottom corner in Figure 4.

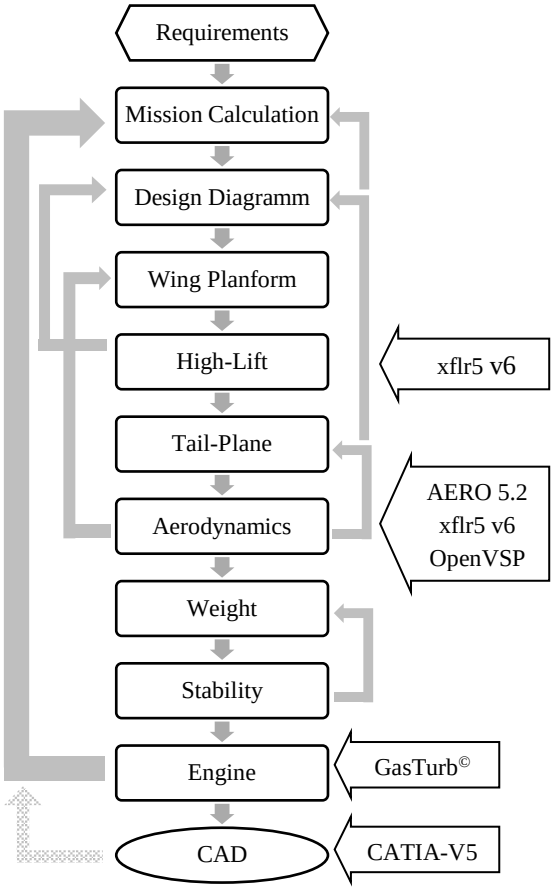

Figure 3. Schematic design process

The lines in this diagram illustrate restraints, which can be either of physical nature like the thrust needed for the desired cruise speed or prescribed by regulations like the approach speed of less than 141 knots (261km/h). [5]

In order to adopt a safety margin to account for inaccuracies of the analytical methods used, the design point was not placed directly on the limitation lines.

The next step is the wing planform where the wing geometry data are calculated, followed by the high-lift section wherein the empirical equations are refined by the software xflr5 v6.

After the tail-plane area prediction, the aerodynamic iteration step is conducted. Herein, values are calculated for every flight segment with the help of the programs AERO 5.2, xflr5 v6 and OpenVSP. The description of the adapted software is presented later in this report. These values can be directly used to refine the mission calculation, the design diagram, the wing planform and the tail-plane area prediction with more precise and reliable data.

Proceeding in the design cycle, the next steps are the weight and stability calculations, creating a small iteration loop.

The last step in the main iteration process is the engine, which is calculated with GasTurb©.

At the end, new calculations are implemented such as take-off noise, sonic boom or emission calculations.

Every formula and software outcome is calibrated either with data from existing, adequate airplanes, papers or books in order to improve the reliability of the results. Calibration means that every empirical method (i.e. mass estimation) is applied to known aircraft and the resulting deviation between method results and actual data is then accounted for accordingly.

The whole iteration process was implemented in Excel with several, mostly manual, interfaces to the programs AERO 5.2, xflr5 v6, GasTurb© and OpenVSP. At a later phase of this study, a 3D model was constructed with the CAD software CATIA-V5 to review the design in terms of structural feasibility and integration of components.

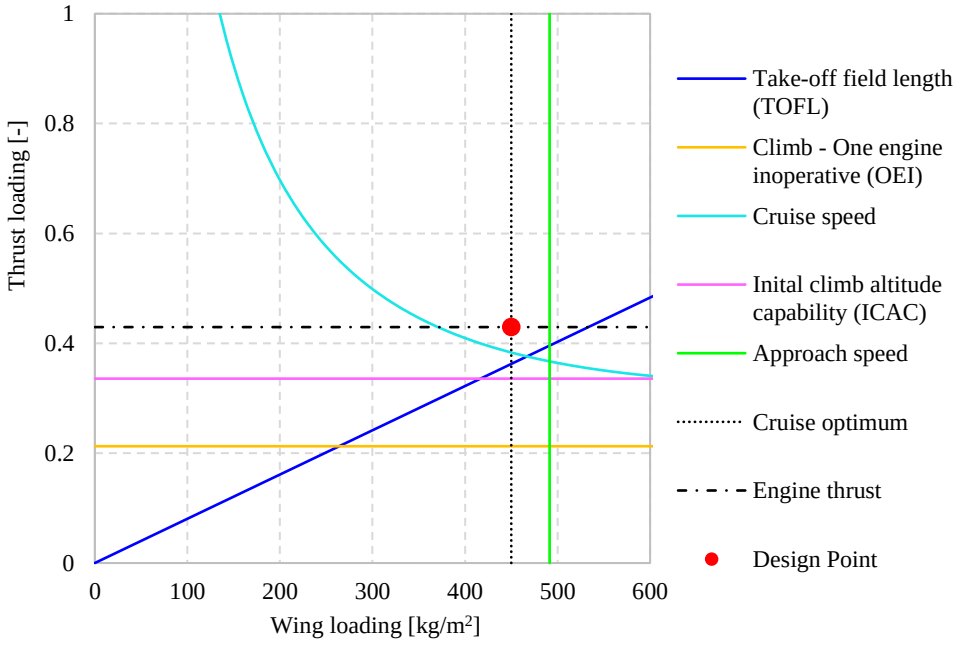

Figure 4. Design diagram

4 The HELESA Design

4.1 Cabin Design

Number of passengers

With an efficient supersonic airplane defined as the main goal, the passenger number has to be as high as possible. This leads to an aircraft with a business-class cabin design instead of one with a business jet cabin design. According to the regulations for large airplanes, CS-25 [6], with up to 19 passengers two emergency exits, one on each side of the fuselage are required. With 20 passengers and more, two emergency exits on each side are prescribed.

The additional doors would cause an increase in weight which would not pay off in terms of efficiency per passenger. So as to avoid an odd passenger number, which would result in a waste of cabin space, the choice fell on 18 passengers for the design case of HELESA.

Passenger Cabin Dimensions

In the supersonic flight regime, the aerodynamic efficiency is highly dependent on the cross-section area distribution and hence on the volume of the aircraft. Therefore, in case of a very large cabin the efficiency would substantially decrease due to increased drag.

The difference in efficiency between configurations with different aisle heights is shown by Horinochi [2]. He calculated a gain in the lift-to-drag ratio of more than 10% for a supersonic business jet with an aisle height of 1.4m compared to 1.8m. Consequently, the cabin dimensions had to be balanced between an aerodynamic efficient design and a size offering enough space to work and travel in a pleasant way. Because the fuselage has a varying diameter, two cross sections are presented in Figure 5, the biggest and the smallest. The smallest, with an aisle height of 1.57m, can be approximately compared with a Learjet 70 [7] and the biggest with an aisle height of 1.7m with a Cessna Citation XLS+ [8]. Furthermore, circular and slightly elliptical cross sections have been adopted to minimize the structural stresses resulting from the pressure difference in high altitudes. The seat pitch is 0,9 m, which is, according to Raymer [9], the upper end of an economy class layout. The aisle width, the emergency exit and the main door are designed in accordance with the European regulations for large airplane CS-25 [6]. The top and side view is shown in Figure 6 and Figure 7.

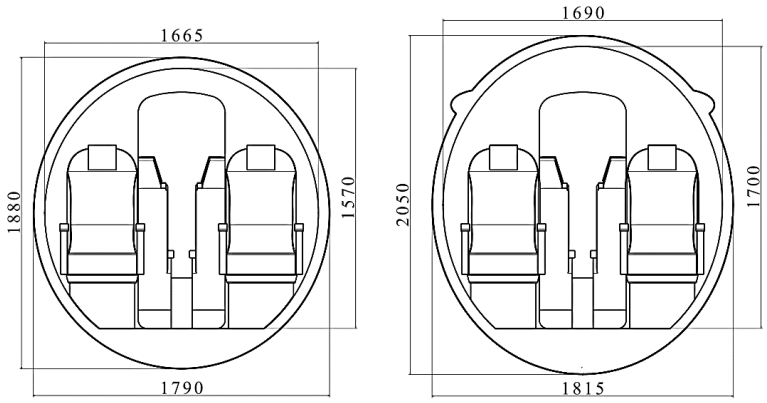

Figure 5. Smallest and biggest cross-section

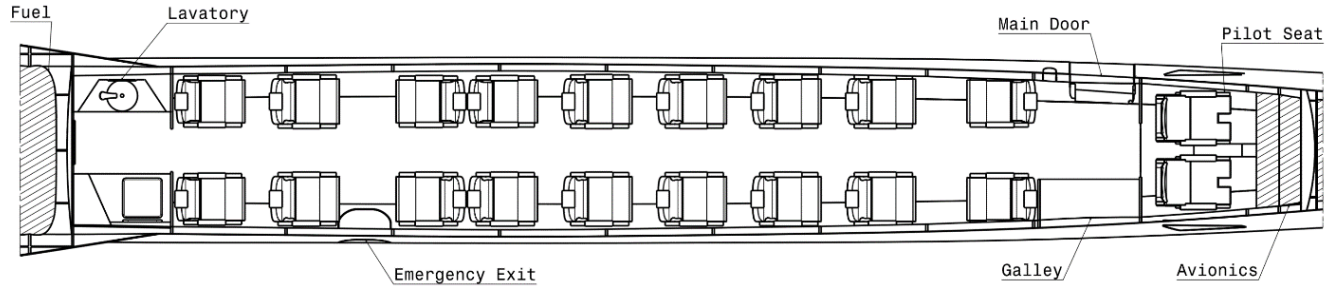

Figure 6. Cabin layout

Windowless Fuselage

In order to minimize structural weight as described in detail in section 4.3.1, windows are avoided with some exceptions, two windows on each side in the cockpit and two further ones in the passenger cabin, in order to comply with safety requirements [4].

The pilots' front view is obtained through an external synthetic vision system, as described by Hartwich et al. [10], with cameras and screens. This allows the nose to be shaped in order to minimize aerodynamic drag without the need of considering the pilots field of sight. For redundancies, the system is equipped with several cameras, transmission systems, backup screens, the left and right windows and a periscope.

To guarantee a high level of comfort and entertainment in the passenger cabin, on each side of the cabin is a row of screens, inspired by the concept of the supersonic business jet design "The Spike S-512" [11]. These screens can be used for personal

entertainment, special light shows or to project the outside view. OLEDs (organic light-emitting diode) are used because of high energy efficiency, lightweight characteristics and flexibility in terms of fitting at the inner cabin wall.

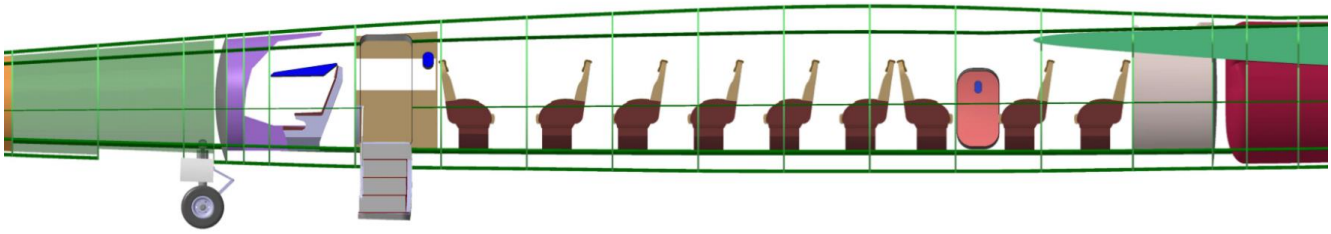

Figure 7. Cabin side view

4.2 Aerodynamics

In this section the fundamentals of different flight regimes, the configuration development for a supersonic aircraft and diverse wing planforms will be discussed. Two studies concerning the empennage and the contradiction between lightweight and aerodynamic efficiency are closing this section.

4.2.1 Subsonic Regime

Since the main part of the climb and descent segments as well as cruise over land are flown with subsonic speeds, it is of great importance to analyze and verify subsonic flight performance.

Sun et al. [12] estimates that the Concorde, having a subsonic L/D of 7, needed 40% of its fuel in the subsonic flight condition. The main reasons were the large wetted area and the high span loading due to the low aspect ratio.

Especially in the HELESA design, where a flexibility between subsonic and supersonic flight is desired, this analysis becomes even more important.

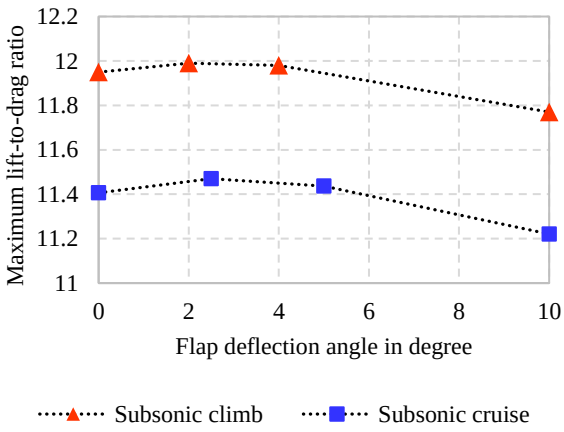

Figure 8. Influence of flap deflection on the lift-to-drag ratio

A variable sweep has the advantage to adapt the wing in terms of sweep angle according to the flying situation. In the subsonic regime, the wing is swept backwards which results in a larger span as well as more relatively thickness compared to the supersonic wing configuration which results in less induced drag. The variable sweep wing will be discussed in detail in section 4.2.4. Because there are different point of views in the literature about the forward swept wing we considered it neither better nor worse besides, according to Raymer [9], the little weight penalty resulting from the untwisting tendency, described in detail in section 4.2.4.

In the climb condition with Mach 0.8, the wing has a forward sweep angle of 35 degree, resulting in a span of 16.1 m. By leaving the wing in the 20-degrees take-off and landing sweep position, the climb would be more fuel efficient but also slower. Whitford [13] describes a 450kg structural weight saving for a conceptional designed F-14 by limiting the sweep angle in climb to 20° up to a Mach number of 0.7. Since the time saving advantage is the main potential of a supersonic aircraft, a higher sweep angle is chosen. Some relevant data for different flight segments are shown in Table 2.

The subsonic drag can be divided in the zero-lift drag and the lift induced drag. The former consists of skin friction, pressure drag, interference, leakage, perturbations and miscellaneous drag. [9]

The drag calculation was calibrated with aerodynamic data from the Boeing 727. Despite the aircraft's age it is used because of a reliable data set.

The zero-lift drag is estimated with the component buildup method according to Raymer [9] wherein the skin friction is calculated with the flat-plate skin-friction coefficient. A full turbulent boundary layer is assumed, due to the difficulties to achieve a laminar boundary layer at high subsonic speeds with relatively thin airfoils and a long slender fuselage.

Additionally, form factors must be considered to include the pressure drag resulting from flow separation.

The lift induced drag is estimated with the 3D-Panel method conducted with AERO 5.2, a software developed at the Institute of Aerodynamics

	Landing	Take-off	Subsonic climb	Transonic cruise	Cut-off cruise	Supersonic climb	Supersonic cruise
Mach number	0.25	0.25	0.8	0.92	1.1	1.2	1.6
Span [m]	18.3	18.3	16.1	14.1	11.2	11.2	11.2
Sweep [°]	20	20	35	45	58	58	58
Max. L/D	4.0	5.9	12.0	11.4	4.6	5.9	7.1

Table 2. Data for different mission segments

and Gas dynamics (IAG) of the University of Stuttgart. Using this tool, it is able to see the influences of minor changes such as flap deflections. Compared to other Boundary Element Methods, the 3D-Panel method is the most sophisticated one factoring in the balancing between accuracy and computational effort.

The compressible effects for the best climbing speed of Mach 0.8 are considered with the Göthert rule, implemented in AERO 5.2.

As a first estimation, NACA 0004 profiles are used at the outer wing, based on the supersonic sweep position, because of the acceptable supersonic performance. To add a chamber for a higher subsonic lift to drag ratio the internally blown plane flaps can be deflected. Estimating the deflection angle as well as the benefit in terms of lift to grad ratio, different flap settings were calculated which is seen in Figure 8.

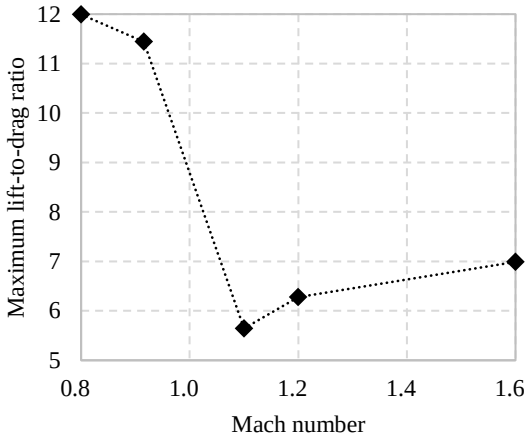

Figure 9. Lift-to-drag ratio against the Mach number

4.2.2 Transonic Regime

The transonic flight condition is defined by the simultaneous occurrence of supersonic and subsonic speed regimes. [14] The cruise at the cutoff Mach number of about 1.1 and the cruise at Mach 0.92. lie within this regime.

In this flight segment drag increases due to the formation of shock waves. This drag rise is visualized in Figure 9 showing the maximum lift-to-drag ratio against the Mach number. It can be led back to the additional wave drag occurring at transonic and supersonic speeds. Wave drag is dependent on the total pressure loss across the shock wave, which is again dependent on the shock wave strength, the shock wave angle and finally the Mach number. At transonic speeds, the shock strength is high which leads to high total pressure losses and consequently to high wave drag. [15]

Due to the increased wave drag the acceleration to supersonic speeds is conducted at an altitude lower than that for cruise. Because the available thrust drops with increasing altitude and decreasing Mach-number, there would not be enough thrust available in higher altitudes to get through the transonic, drag intensive regime. Therefore, if accelerating at about 11 km altitude, enough thrust would still be available to accelerate to supersonic speeds before climbing further exploiting the higher thrust level due to the ram effect.

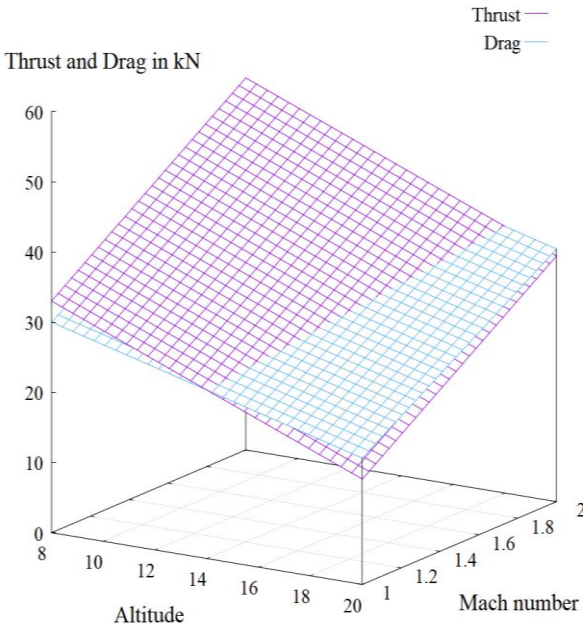

Figure 10. Thrust and drag against Mach number and altitude

In order to visualize this, the available thrust and the drag are plotted against the Mach number and the altitude in Figure 10. This diagram is obtained by calculating the values at the corners and interpolating the remaining data linearly. The intersection of these two surfaces presents the limit of horizontal flight in terms of altitude and Mach number.

An interesting phenomenon while accelerating from subsonic through transonic to supersonic speeds is the backwards movement of the aerodynamic center being discussed in section 4.3.2.

4.2.3 Supersonic Regime

The supersonic flight regime differs from the subsonic basically by the additional wave drag, containing of volume and lift dependent wave drag. The drag breakdown is shown without the trim drag according to Torenbeek [16] in Figure 11. The form and the interference drag are included into the volume dependent wave drag. The drag coefficients are represented in Figure 12 for the supersonic (Ma=1.6) and transonic (Ma=1.1) regime in terms of best range conditions and for subsonic (Ma=0.8) speeds according to the fastest vertical speed. As can be seen, in the subsonic condition, the wave drag has vanished whereas interference drag and form drag occurs.

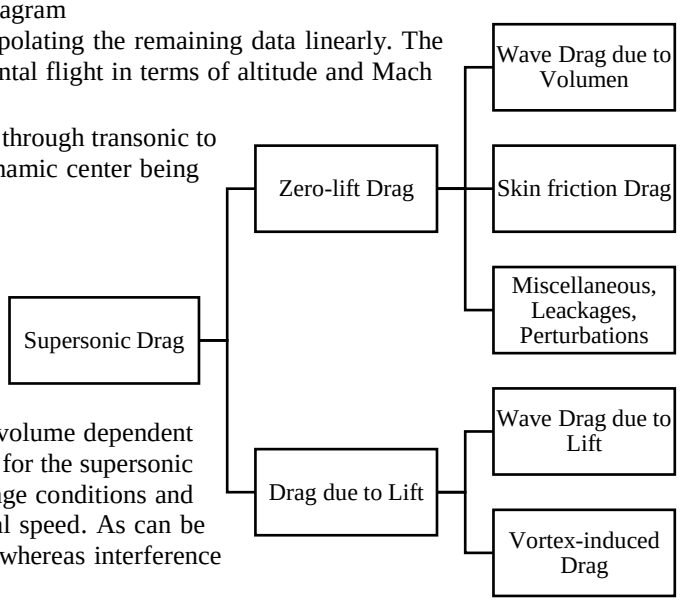

Figure 11. Supersonic drag breakdown [42]

In the following lines, the main drag components are described regarding the calculation methods and how they can be minimized.

Skin friction Drag

The skin friction drag is calculated with the flat-plate skin-friction coefficient, described by Raymer [9]. This skin-friction coefficient is dependent at the Reynolds number and whether the boundary layer is laminar or turbulent. [17]

The laminar boundary layer is in general an unstable condition especially at high Reynolds-numbers [18]. However, it can be obtained either by an active boundary layer control with surface suction or cooling or by special passive measures. The first mentioned has weight and complexity penalties and has never applied at an aircraft before which is why the feasibility of a natural laminar flow is discussed below.

The compressibility effect serves as kind of a stabilizer. Mack [19] compared different transition measurements with the stability theory. He concluded that the transition Reynolds-number, after decreasing from Mach 0 to the transonic regime, rises again with almost no differences between Mach 1.3 and 1.8 but a slight maximum at about Mach 1.6. It can therefore be concluded that natural laminar distances in supersonic flight are possible.

Sturdza [20] calculates a halving of the maximum takeoff weight by increasing the wings natural laminar flow fraction from 10% to 80%. This indicates the potential of the supersonic laminar boundary layer which is why the main three concepts are introduced:

a) The best known is the natural laminar flow wing patented by Tracy [21]. The concept is to minimize the sweep angle resulting in a supersonic leading-edge and a reduction of the cross flow which disturbs the laminar boundary layer. Because of the supersonic leading-edge, it is possible to implement big pressure gradients in stream wise direction which stabilizes the laminar boundary layer. This natural laminar flow wing was successfully tested in flight with a F-104 in 1959 [22] and a F-15B in 1999 [23] by NASA and is also applied at the supersonic business jet design from AERION Corporation, which shall entry into service in 2023 [24].

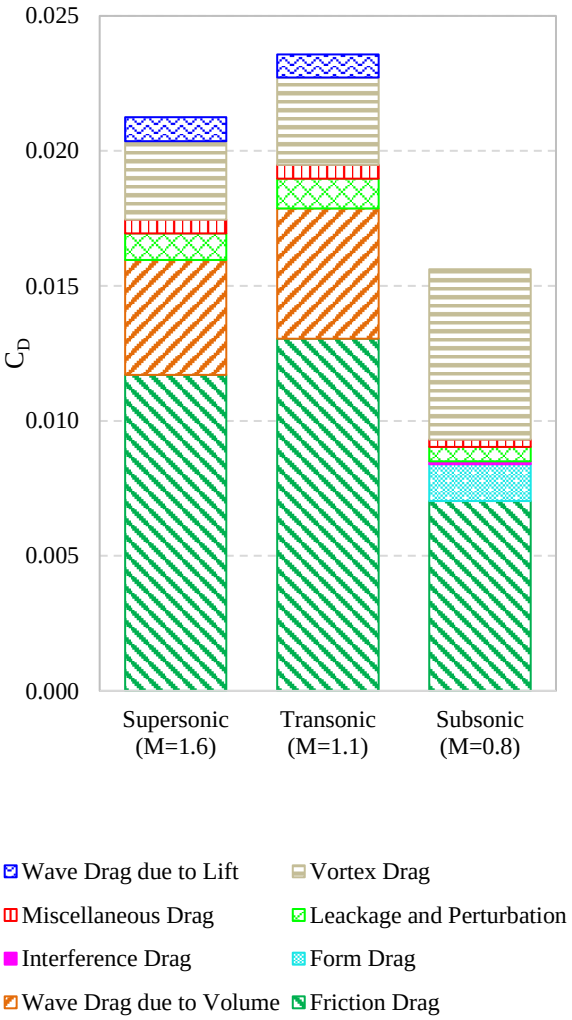

Figure 12. Drag coefficients at supersonic and transonic cruise and subsonic climb

b) A further possibility might be the concept examined by the scaled unmanned national experimental supersonic transport project (NEXST-1) conducted by the Japan Aerospace Exploration Agency (JAXA) [25]. They are investigating, among many other drag reducing technologies, the natural laminar flow wing with a subsonic leading-edge in supersonic flight. For wings with sweep angles larger than the critical one, the crossflow instabilities, taking place near the leading-edge, have the major influence on the laminar-turbulent transition [26]. This cross flow is generated by the pressure gradient in chord wise direction which is why a high pressure gradient on the upper surface on a very small distance at the leading-edge followed by a flat top pressure distribution is designed. Several wind tunnel tests and a flying test with an unmanned scaled airplane proofed the operability [27]. Although this concept just works on the upper surface, the combination between high sweep angles and a laminar boundary-layer portion demonstrates great potential.

c) The last option is the distributed roughness concept investigated by Saric and Reed [28]. It works by stimulating waves with a distributed roughness parallel to the leading-edge which counteract the crossflow instabilities. Although wind tunnel tests proved the reliability of this method, further work will be done, “concentrating on optimization of roughness diameter and spacing for laminar flow control and extending the work to higher Reynolds numbers” [28].

Because of the combination of a subsonic leading-edge with a laminar boundary layer and the more advanced technology readiness level compared to the distributed roughness concept, the method investigated by the JAXA has been used. Assuming a 40% laminar boundary layer fraction for the supersonic cruise condition on the upper surface of the outer variable wing, which is a reasonable value [27], the maximum take-off weight was reduced by 4.1%.

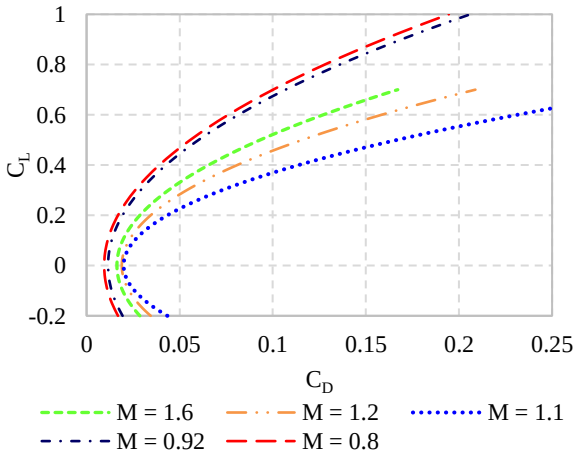

Figure 13. Drag polar for different mission segments

Because of the different flight condition at the supersonic climb, just 10% laminar boundary fraction was assumed.
The calculated values were calibrated with data from a conceptual designed supersonic business jet by Schuermann [29].

Wave Drag

The wave drag is caused by the formation of shock waves and the associated total pressure loss. [15]
Von Kármán [30], Haack [31] and Sears [32] were the first to calculate the wave drag of slender bodies of revolution in supersonic flow. They defined the shape of such projectiles for the minimum wave drag of a given volume and diameter. After that, Whitcomb [33] wrote down the "Area Rule" which says, that the wave drag of a wing body combination at transonic speed is almost the same as the drag of an equivalent body of revolution with the identical cross-sectional area distribution. Jones [34] expanded this theory to supersonic speeds. In the transonic area rule, the cutting planes are located perpendicular to the stream leading to one cross section per longitudinal position. In Jones theory, the cutting planes are inclined at the Mach angle μ which equals $\sin^{-1}(1/Ma_\infty)$ and turned at every possible angle θ around the longitudinal axis of the aircraft resulting in an infinite number of planes for every longitudinal position. Therefore, every angle θ has an individual cross-sectional distribution and consequently a wave drag value. Lomax [35] later presented the complete linearized theory for the supersonic area rule, including the lift dependent term, seen in equation (4-1).

$$\frac{\mathrm{D}}{\mathrm{q}} = -\frac{1}{4\pi^2}\int_0^{2\pi}\int_0^{L^*}\int_0^{L^*}\left\{A''(x_1,\theta)-\frac{\beta}{2q}l'(x_1,\theta)\right\}\left\{A''(x_2,\theta)-\frac{\beta}{2q}l'(x_2,\theta)\right\}\log_e|x_1-x_2|\,dx_1dx_2d\theta \qquad (4\text{-}1)$$

Harris [36] published 1964 a computer program which was made leaner by McCullers [37] 1992, called AWAVE. To overcome geometry input inaccuracies of these tools, the geometry generation tool provided by OpenVSP is combined with the volume dependent wave drag calculation by Waddington [38]. The comparison with this tool and the exact solution of a Sears-Haack body resulted in an error of below 0.01% if more than 10 cutting planes are used [38]. The comparison with an Eminton and Lord body [39] which is an axially symmetric body with approximately the same cross-sectional area distribution of a fuselage with a backward swept wing, resulted in an error of less than 1% for more than 34 slices [38].

The use of this tool in the conceptual design phase is excellent because of the quick results and the visual feedback which allows geometrical adjustments. Because this tool provides just a solution for the wave drag due to volume, an additional program was written on basis of the geometry data from OpenVSP to calculate the wave drag due to lift. As seen in the second term in the curly brackets in equation (4-1), the wave drag due to lift is dependent on the first derivation with respect to x of the longitudinal distribution of the lift $l'(x,\theta)$. Because of the lack of knowledge of the longitudinal lift distribution, the needed lift was distributed with respect to the cross-sectional areas of the wing. In order to minimize lift-dependent wave drag a smooth longitudinal lift distribution with no steep lift rises along the whole aircraft is desirable.

Summarizing, there are two equivalent bodies, due to lift and due to volume, which contribute to the total wave drag and to the sonic boom formation. Two examples of the cross-sectional area distribution for Mach 1.6 and a lift coefficient of 0.14 are presented with an angle θ of 0° and 135° in Figure 14 and Figure 15.

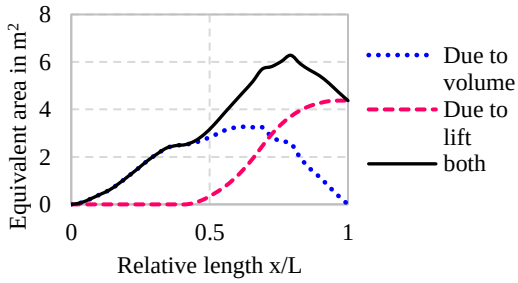

Figure 14. Equivalent bodies for the angle θ of 0°

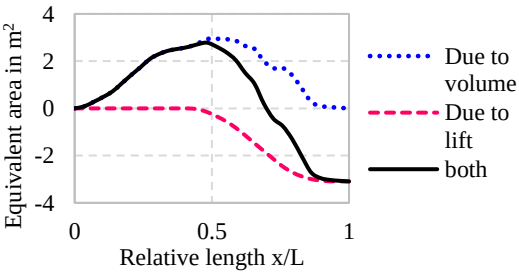

Figure 15. Equivalent bodies for the angle θ of 135°

In order to minimize wave drag due to volume, as much as possible cross-sectional area distributions were converged with the Sears-Haack body which is the body with minimum wave drag for a given volume. The von Kármán Ogive, which is optimized for a given diameter with a finite base area was not applied because the maximum diameter of the fuselage was minimized to an extent where the needed volume for fuel, passenger and systems became the critical parameter.

The lift-dependent wave drag was reduced by ensuring a smooth lift distribution in the longitudinal direction. This results in a long wing root, which must be balanced off against a sufficient outer wing area for high lift and stability purposes on the one hand and for high wing loading on the other. Furthermore, the intersection of the wing root with the cabin should be avoided because of structural weight penalty reasons.

Concluding this section, minimization in wave drag should not be considered without taking into account the skin friction, structural weight and operability in terms of turnaround or landing gear position and compartment. Therefore, investigations concerning these parameters are conducted in section 4.2.6.

4.2.4 The Wing

Since the wing is the most important configuration parameter for supersonic airplanes, a configuration matrix was developed, shown in Table 3. Each wing type obtains score ranging from -3 to 3 for every characteristic, which are then weighted according to their importance.

The variable-sweep, forward-swept wing achieved the highest score, followed by the cranked delta and the tapered wing with strakes.

These wing types are discussed subsequently in order to explain the different assessments.

Parameters	**Structural weight**	**Aero-elastic performance**	**Stalling properties**	**Aero. center movement**	**Supersonic efficiency**	**Subsonic efficiency**	**High lift potential**	**Fuel volume**	***Result***
Weighting	*10%*	*5%*	*5%*	*10%*	*30%*	*20%*	*15%*	*5%*	
Delta wing	1	2	2	2	1	-2	-2	2	***0.20***
Tapered wing	0	0	0	-1	-2	0	1	1	***-0.50***
Tapered wing with strakes	0	1	2	1	1	-1	1	1	***0.55***
Cranked delta wing	1	2	2	2	1.5	-1	0	2	***0.85***
Natural laminar flow wing	-1	0	0	-1	1	-1	0	0	***-0.1***
Supersonic bi-plane	3	2	0	-1	1	-2	1	0	***0.35***
Forward swept wing	-2	-3	3	0	1	1	1	0	***0.45***
Backward variable sweep	-2	0	0	-2	1	1	3	-2	***0.45***
Forward variable sweep	-2	-3	3	3	1	1	3	-2	***0.95***

Table 3. Wing configuration matrix

The Delta Wing

The delta wing has a planform of a triangle with the tip in the flying direction. Because of the long root chord, relatively thin profiles can be used combining the advantage of high sweep angles and thin profiles. Typically, the wing has a low aspect ratio, which has structural and aero elastic benefits. Furthermore, the delta wing neither stalls abruptly nor has the tendency for nose diving. The movement of the aerodynamic center is, measured in percentage of the mean aerodynamic chord, relatively small.

A special configuration is the all-flying tail where the horizontal tail is merged with the wing and the ailerons are combined with the elevators, called elevons. This has the advantage of lower interference drag but leads to a larger potential horizontal tail area caused by the shorter moment arm. The result is a higher trim drag and a lower maximum lift coefficient. In order to maintain an adequate approach speed the wing area should be increased, which leads to higher weight and more skin friction. Experiments with a horizontal tail were not satisfying because of the large downwind resulting from the low aspect ratio. [40]

A promising alternative could be the canard which leads to higher maximum lift coefficients and better longitudinal static and dynamic stability. [40]

Nevertheless, the high span loading resulting in a high induced drag in subsonic flight does not meet the requirements of having an airplane which can operate flexibly in supersonic and subsonic flight conditions.

Tapered Wing with Strake and the cranked Delta Wing

To achieve a compromise between subsonic and supersonic efficiency, a combination of a highly swept delta wing, the strake in combination with a lower swept tapered wing is an option, such as that of the McDonnell Douglas F-18 [41]. At high

angles of attack the strake causes vortexes on the upper inner part of the wing. This stabilizes the flow and delays the stall. Compared to a pure tapered wing it provides reduced wave drag because of the higher sweep angle of the inner wing as well as better high lift performance. The trim drag also decreases because the aerodynamic center does not move that far back as for a tapered wing during the transition from subsonic to supersonic speeds. The cranked delta wing, consisting basically of two delta wings, has comparable properties as the strake wing but still less wave drag as well as trim drag [41]. The cranked delta wing could be a possibility for the HELESA design, but the subsonic aerodynamic inefficiency would be a significant disadvantage.

Supersonic natural laminar flow wing

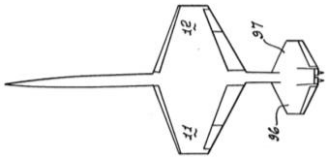

Figure 16. Supersonic laminar flow wing by Tracy [18]

The concept of this wing is to minimize the cross flow by reducing the sweep angle resulting in a supersonic leading-edge being used to generate high pressure gradients in stream wise direction [42]. This wing type has already been tested successfully by the NASA and AERION Corporation are implementing it in their supersonic business jet design. [24]

Its main advantage is the significantly reduced skin friction drag because of the higher laminar-turbulent boundary layer fraction. The lower sweep angle is also positive in terms of crossflow in the subsonic flight regime, however the sharp leading-edge and the thin profiles are challenging features. The high lift potential is limited by the early separation of the flow due to the mentioned sharp leading-edge which could be resolved with a slat. The thin profiles increase the structural weight and reduce the volume for fuel in the wing.

The wave drag due to volume is affected, considering the theory of Jones [34], by the cross-sectional distribution. Imagining the cutting planes for the angle θ near 0° or 180°, assuming 0° is the normal flight condition, the transition of the fuselage and wing is sharp and therefore hard to be fully balanced by the fuselage shape. This results in higher wave drag compared to a conventional high swept wing, whereas the transition at angles θ of about 90° and 270° is smoother which should compensate the first mentioned higher wave drag. The problem hereby is the deviation of the higher aspect ratio laminar flow wing configuration from an axisymmetric body. The total wave drag due to volume is a result of the cross-sectional distribution of every angle θ. Hence, the higher this deviation, the harder it is to fulfill the optimum cross-sectional distribution for every angle θ.

Furthermore, the wave drag due to lift is highly dependent on the first derivation with respect to x of the longitudinal lift distribution according to Lomax [35]. The higher aspect ratio of the laminar flow wing results in a short peak and a steep rise in this lift distribution which leads to a higher wave drag due to lift. In addition, this sharp longitudinal lift distribution strongly increases the sonic boom. Although the low sonic boom was not the design case, it was chosen not to go for a configuration with which it is probably impossible to fulfill the low boom requirements.

Sturdza [20] compared this low sweep natural flow wing with a cranked delta wing configuration. It results in 14% lower total zero lift drag even though the inviscid drag, basically the wave drag, of the laminar flow wing configuration is four times as high. This meets the previously mentioned considerations. He also writes, that this “crude comparison” [20] should be done more carefully considering the fact that the laminar flow design is the result of a multidisciplinary design study compared to the cranked arrow wing.

The supersonic Biplane

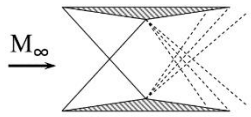

Figure 17. Busemann bi-plane [143]

The biplane was first presented by A. Busemann at the fifth Volta congress in Rome in 1935. He presented the famous paper [43], in which he explained the advantages of a swept wing. At the end of this congress, he presented a wave drag canceling biplane, the Busemann wing.

The wave drag due to lift is reduced by the *wave-reduction effect*. A flat plate airfoil with an angle of attack of α and n flat plate airfoils with an angle of attack of α_s, installed on top of each other with the same chord length and overall lift is compared. Applying the 2-D supersonic thin airfoil theory [44], the angle of attack has the relation $\alpha = \alpha_s/n$ and the wave drag due to lift of the n plates is proportional to $1/n$ compared to the single flat plate. Indeed, the skin friction drag must be considered, which is proportional to n. [45]

The wave drag due to thickness or volume is reduced by the *wave cancellation effect*. By locating two airfoils in the adequate position, the shock waves can be canceled out which results, theoretically, at small angles of attacks in the same lift and drag conditions as a thin flat plate by applying the thin airfoil theory [44]. In reality, the entropy production caused by the shock waves between the wings and a larger wetted area cause more drag. [46]

Licher [47] designed an unsymmetrical biplane which combines the wave-reduction and the wave cancellation effect under constant lift conditions. The wave drag due to thickness is almost canceled out and the wave drag due to lift is reduced by 2/3 of that of a flat plate at the same lifting conditions. [48]

There are many further optimizations of the basic Busemann biplane, mostly conducted through an inverse problem approach. The big issue of a supersonic biplane is the off-design condition. By accelerating, the biplane chocks, which comes clear by comparing it with a supersonic inlet diffuser [49]. Reaching Mach 1, the ratio of throat area to inlet area must be one. By further acceleration, this ratio must become less in a special manner, so as to avoid chocking.

Therefore, if a fixed biplane is applied, a hysteresis effect occurs leading to high transonic drag, higher than for a diamond airfoil and furthermore, the need of accelerating to a much higher Mach number and subsequently decelerate to the cruise Mach number, to achieve the optimum shock wave pattern between the biplane. [46]

To cope with this problem, flaps could be applied at the leading-edge, to alter the inlet to throat area ratio. In addition, flaps at the trailing-edge can be used to increase the chamber for subsonic flight as well as for high lift purposes. A study analyzed the application of flaps on a biplane [50]. The results showed a reduction of the transonic drag and of the hysteresis effect compared to a fixed Busemann biplane. Nevertheless, by looking at the results of this study, the Busemann biplane with deflected leading-edge flaps has still higher transonic drag and just slightly less drag at the design Mach number than the diamond airfoil, although these were inviscid calculations. These results were also calculated by other studies [51] [52]. Applying this concept to a real aircraft, the little less drag in the design Mach number could be disappear by adding the additional skin friction drag of the biplane and the weight, higher wetted area and bigger volume of the larger engine, needed to cross the transonic regime.

Certainly, there is an advantage in wing structural weight, but the proposed advantages in terms of drag reduction might not be achieved. Although a high lift coefficient of up to 2 for the airfoil with leading-edge and trailing edge flaps can be reached [46], the high subsonic cruise, which was one of the HELESA design goals, would be inefficient because of sharp leading-edges, higher wetted area and perhaps a ram effect.

Concluding this section, the optimized Busemann biplane with flaps has potential for a low boom aircraft, however this solution might not be suited for a fuel-efficient design, mostly due to the hysteresis effects.

The variable-sweep Wing

The variable swept wing offers good aerodynamic efficiency both in subsonic and supersonic flight [41]. It is possible to adapt the sweep angle and the associated aspect ratio as well as the relative airfoil thickness, measured in stream wise direction.

The variable wing comes from military requirements of flying long range subsonic cruise or loiter, flying at supersonic speeds and operate from airports with limited runway lengths [13]. These requirements have several similarities to the current design goal.

Beside the subsonic and supersonic efficiencies, the take-off and landing performance is better than that of other fixed supersonic wings, because of the lower sweep angle as well as the higher flap effectiveness and the bigger relative airfoil thickness, which relates the stall and enables the use of effective slats and slotted flaps.

The major disadvantage is the weight penalty due to the complex mechanical sweeping mechanism. However, there is also a weight saving potential caused by the likely smaller wing area as well as the lower thrust to weight ratio and, assuming a constant high lift coefficient, a less complex high lift system. In addition, the smaller wing generates less skin friction drag especially in the supersonic flight regime, which again reduces the amount of required fuel and consequently the structural weight.

Thus, if the mission fits to this type of wing, there could be no or even positive weight effects. In order to analyze this phenomenon, Grumman has built two test aircraft for the development of the F-14, one with fixed wings and one with variable sweep. The result was a weight saving of the variable swept wing configuration of almost 2,250kg [13]. Furthermore, even with a double-slotted flap system, the fixed wing version 303F could not meet the wave-off (go around) rate of climb regulation [13]. To be fair, the requirements of a naval aircraft for aircraft carrier are advanced and predestined for the variable sweep wing, but they are not that far away.

Another disadvantage is the reduced volume available for fuel because of the variable sweep mechanism and the space for the part of the retracted wing.

Forward-swept versus backward-swept

A disadvantage of a forward-swept wing is the increased structural weight by the aero elastic tailoring effect. By bending a forward-swept wing upwards, the wing tips twist in an angle of attack increasing way, which increases the wing tip loading. Subsequently the wing bends more resulting in more loading. This is a significant drawback if constructing the wing with aluminum, but by exploiting the possibility with fiber composite materials of high stiffness and adjusting them differently in different directions, there could be just a “minimal weight penalty”. [9]

The natural directional stability is affected by the negative dihedral effect from the forward swept wing, which must be counteracted by a higher dihedral position. [9]

The fact that the wing root of a forward swept wing is closer to the rear of the plane causes a higher pitching moment when flaps are deflected, but also has the advantage, that the wing box can be placed, behind the cabin especially for a small business jet. The hinge line of a forward swept wing is more swept than a backwards swept, which decreases the high lift potential. [9]

Moving on to the advantages, the forward swept wing has better stall properties compared to a backwards swept one, because it first stalls near the root, allowing aileron control at stall conditions. [9]. The reason why the forward swept first stalls at the root is amongst others the crossflow from the tip to the root. This could be a disadvantage especially for this aircraft, which has an inner backward and an outer forward swept wing. This would lead to a collision of the cross flows and

subsequently the first stall at the kink between these two wing parts. The wake of this stall region could hit the V-Tail which would reduce the maneuverability. But because of the lower sweep angle of the outer variable wing at landing and take-off conditions, the crossflow should not be that distinctive and the flaps have also an influence on the stall location. This phenomenon must be investigated in future work.

As already mentioned in section 4.2.3, the forward swept wing has advantages in terms of lift dependent wave drag, because the longitudinal lift distribution is smoother, especially at θ angles near 90° and 270°.

Comparing a backward-swept and a forward-swept wing with the same leading-edge sweep angle at high subsonic flow, the angle of the shock wave on top of the wing is higher for the forward-swept wing, which results in lower transonic wave drag. Assuming the same shock angle, the forward swept has still the advantage of a lower leading-edge sweep, which leads to a lower structural weight penalty and induced drag as well as better high lift properties [13]. In addition, the bending moment at the pivot point can be reduced by approximately 12% compared to a backwards variable swept wing with the same wing area, taper ratio, aspect ratio and shock sweep [53]. This could minimize the weight penalty described previously.

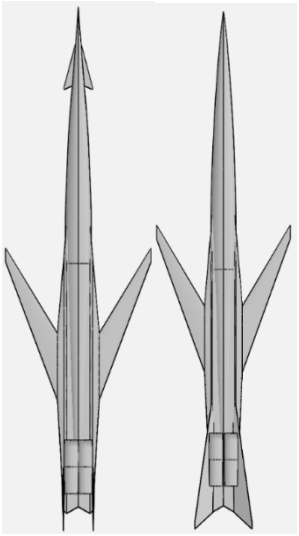

Figure 18. Geometries of the tail-plane design study

Because it is hard to trade the advantages against the disadvantages, we will have a look at some investigations. Raymer [9] writes that his "experience in numerous design studies is that forward sweep, integrated into a real aircraft design, usually has higher supersonic drag". Nevertheless, test data measured by the NASA [54] with an experimental aircraft from Grumman, the X-29A, in a range of Mach 0.4 to 1.3 will be discussed. The data were compared with three other contemporary fighter aircraft, the F-15C, the F-16C and the F/A-18. The results showed, that the lift-to-drag ratio of the X-29A is slightly lower in the subsonic and transonic regime whereas at Mach 1.3 it is approximately the same as the averaged value of the other three aircraft. The zero lift drag of the X-29A is in every flight regime, especially in the supersonic, higher. This could be the result of the underwing actuator fairing for the automatic camber control, which was tested in another investigation.

Concluding this section, the fixed forward swept wing probably has neither significant advantages nor disadvantages. However, assuming the same aerodynamic characteristics as a backward-swept wing, a further decisive advantage is the reduction of the trim drag in supersonic flight by counteracting the aerodynamic center movement while transitioning from the subsonic to the supersonic flight regime, described in more detail in section 4.3.2.

4.2.5 Canard versus V-Tail

Two potential tail-plane options were analyzed, the canard with two vertical tails and a V-tail. Two vertical tails are used because of the need of shielding the jet noise whilst of course providing directional stability. Neither the geometry in Figure 18 nor the presented data in Table 4 are representative of the final design, because this study was conducted at an early stage of the design process. The tail areas were calculated with the "Tail volume coefficient" method according to Raymer [9] and calibrated with an average volume coefficient, taken from several supersonic bomber aircraft. The V-Tail area was not calculated with the optimum theoreticaly theory, which would have resulted in a smaller area, but by summing the two imaginary vertical and horizontal tail areas up as recommended by Purser and Campbell, [55].

	Canard	V-Tail
MTOM	40,180kg	39,950kg
OME	19,800kg	19,300kg
Fuel Weight	18,480kg	18,750kg
Fuel Efficiency	8.36 pkm/kg	8.31 pkm/kg
L/D	7.2	7.1

Table 4. Data from the tail-configuration comparison

The requirements were the same for both configurations. The results in Table 4 shows a slightly heavier structural mass for the canard version which is caused by the higher bending moment on the fuselage, resulting from the longer moment arm between center of gravity and the center of pressure of the canard. The lower fuel weight of the canard version derives from the smaller wetted area, caused from the mentioned longer moment arm. The lift dependent wave drag is marginally lower for the canard version because of the better longitudinal lift distribution. Therefore, the V-Tail has a slightly lower maximum takeoff mass, whereas the canard has a higher lift-to-drag ratio. Looking at the efficiency in terms of passenger kilometers per kg fuel, there is almost no difference. This leads to the application of the V-tail version, considering the better noise shielding characteristics, because the V-Tail area is bigger than the vertical tail area of the canard version.

4.2.6 Aerodynamic Efficiency versus Structural Mass

This analysis was basically conducted to identify the optimum fuselage length. By increasing the fuselage length, the wave drag decreases, but the structural mass increases as well as the wetted area and therefore the skin friction drag. There is an optimum between these three parameters, which is the goal of this analysis. Again, the presented study was conducted in an early stage of the design process. Five versions were designed having a fuselage length of 35m, 38m, 40m, 42m, and 45m. The constant values, to gain a reasonable basis of comparison, are the ratio of inner to outer wing area, wing loading, thrust

loading, fuselage volume and fuselage maximum diameter. Furthermore, this study just considers supersonic cruise at Mach 1.6.

The relevant value is the efficiency expressed in passenger km per kg fuel. As seen in Figure 19, the efficiency has a peak at a length of 40m, whereas the maximum lift-to-drag ratio has its maximum at 42m length resulting from the increasing maximum take-off mass. This can be visualized by imagining the distance between the MTOM and the L/D graph in Figure 19. This leads to a fuselage length of 41m and a fineness ratio of 22.

Having just considered the skin friction and wave drag, Dubs [40] describes an optimum of a fineness ratio of 16. If considering the additional structural mass resulting from the current lower fineness ratio, Dubs' fineness ratio should become even less.

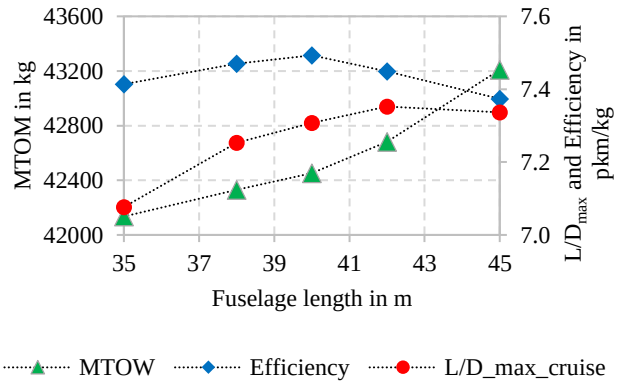

Figure 19. Optimization of the fuselage length

Nevertheless, the calculated results were applied, because of the lack of detail in Dubs' data as well as the many other influences on this comparison.

In Figure 20, the behavior of the MTOM and the fuselage mass with an increasing fuselage length is shown. It can be noticed, that the fuselage mass increases almost linearly, whereas the MTOM increases more in an exponential way, just as expected.

Further considerations concerning the operability and landing gear placements should be made.

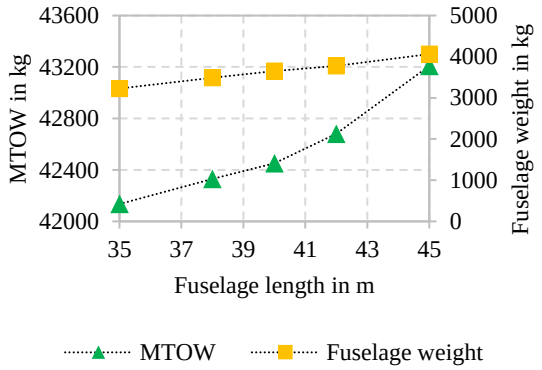

Figure 20. Fuselage length versus MTOM and fuselage weight

4.2.7 Wave Rider

As described in section 4.2.4 the original consideration behind the Busemann biplane was to use it as a wing. The advantage would be a reduction in wave drag. However, while showing excellent performance at design Mach number, hysteresis and choking effects occur at off-design [56] [57] [58].

According to Gerhardt [59], in this configuration, the aim was to implement the Busemann biplane as a compression lift by performing a 90-degree rotation and placing it under the aft section of the fuselage whereby additional lift at supersonic cruise is produced. Due to the wave-cancellation-effect, wave-drag due to volume is reduced while the generated shock waves produce high pressure leading to a force component vertical to the fuselages bottom.

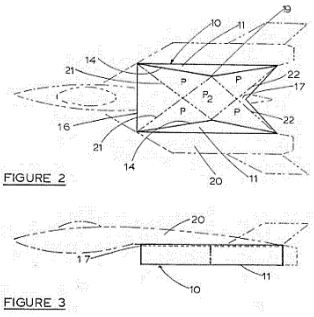

Figure 21. Lifting shock wave cancellation module [56]

To evaluate the benefit, analytical and computational analysis were performed. The analytical and computational two-dimensional results in Appendix I, Figure 35, showed a broad consensus and promised lift-to-drag ratios between 18.6 to 20.4 which would lead to an increase of 8% in overall fuel efficiency. However, three-dimensional CFD studies revealed that effects such as edge vortices lead to a blow out of the overpressure seen in Appendix I, Figure 36, which reduces the lift-to-drag ratio to 3.5.

This results in excluding this concept despite the conducted CFD analyzes.

In further studies, it would be interesting to investigate the influence of a slightly downwards directed tail to hold the pressure, produced by the configuration, similar to a wave rider. In this case, the occurrence of a top-heavy moment can cause problems in longitudinal stability.

4.3 Mass Prediction and Stability

The mass and the static stability are two important and highly connected subjects which are subsequently discussed.

4.3.1 Mass Prediction

Materials of the Structure

The possible materials for the fuselage, the wing, the empenage, and the nacelle are aluminium alloys, fiber-reinforced polymers or titanium alloys. Because of the higher specific strength and the possibility of easyer realization of complex shapes carbon or in some crash critical parts aramid fiber reinforced materials are applied. The peak temperature is less than 65 °C at Mach 1.6 as reported by Horinouchi [2]. Recalculating the temperature according to "Schlichting und Truckenbrodt"

[60] resulted in a peak temperature of 55°C and a wall temperature due to friction of 37°C. Since even subsonic aircraft are designwd for temperatures from -55 to +80 °C [61] the aerodynamic heating is not an issue.

Manufacturing Methods

In order to cope with the complex shape of the fuselage, the winding method around a core is used. The core can be partly removed throug the door or the open nose section. The stringers are manufactured by implementing rovings in longitudinal notches in the core. The spars are halfwise triaxial braided around a foam core and subsequently installed.

The wings and the tail-planes are manufactured in the standard way with two half-shells which are then glued together.

Contemporary rules prescribe, that the primary structures need to be secured in addition to the adhesive bonding by rivets, because of the lack of reliable non-destructive testing techniques. Consistent adhesive bonding would result in a stronger undisturbed highly integrated structure. Nevertheless, despite the effort in developing non-destructive testing methods the primary structure is also secured by rivets to minimize risk.

Mass Prediction

The mass prediction of almost all structures and components was realized by using empirical formulas from Raymer [9], Torenbeek [62] and Roskam [63]. These were calibrated with an appropriate reference airplane in order to obtain more reliable values. This is realized by calculating the mass with three to five different formulas for each aircraft element and subsequently comparing the results with the reference value. The equation which provides the lowest result deviation is applied. This deviation is then accounted for through a calibration factor. Furthermore, factors according to Raymer [9] were used on the fuselage, wing, tail, nacelle and landing gear to consider the effect of advanced lightweight materials.

Table 5 shows the calculated masses with their corresponding reference airplanes and literature.

Item	Mass in kg	Ref. Aircraft	Ref. Literature
Fuselage	3,270	*(3)*	[62]
Inner Wing	1,026	*(3)*	[9]
Outer Wing	1,390	*(3)*	[9]
V-Tail	378	*(3)*	[63]
Main Landing gear	1,163	*(2)*	[62]
Nose Landing gear	174	*(2)*	[62]
Nacelle	796	*(2)*	[9]
Engine (one)	1,800	*(4)*	[65] [66]
Fuel system	954	*(1)*	[9]
Starter system	154	*(1)*	[63]
Engine controls	31	*(1)*	[63]
Oil system & cooler	47	*(1)*	[63]
Ducting system (Flaps)	59	-	[69] [70]

Item	Mass in kg	Ref. Aircraft	Ref. Literature
Air conditioning	599	*(2)*	[62]
Piezoelectric De-icing	15	*(2)*	[64]
Electrical system	706	*(2)*	[62]
Hydraulics & pneumatics	394	*(2)*	[62]
Surface Control	600	*(2)*	[62]
Avionics	626	*(2)*	[9]
Fixed interior	1,865	*(2)*	[62]
Operating items	479	*(2)*	[62]
Battery	175	-	[67]
EGTS	323	-	[66] [68]
Variable sweep mechanism	300	-	-
Miscellaneous	10	-	-

Table 5. Component masses

(1) Boeing 737-200
(2) Gulfstream American
(3) Supersonic Business Jet [29]
(4) GasTurb©

Special considerations were made for the outer wing. Because it is swept forward, further 10% in mass is assumed. For the inner and outer wing, 19% more mass was added according to Raymer [9], to take into account the structural reinforcement required by the variable sweep. The fuselage is constructed with almost no windows which allows to manufacture the fuselage with less reinforcement near the windows leading to an estimated mass reduction of 2% of the total fuselage mass. The air-conditioning system is assumed to be 100% heavier than a conventional one because of the required electrical compressors (More Electric Aircraft). Instead of an auxiliary power unit (APU), an advanced Lithium-Sulfur battery system with an energy density of 600 Wh/kg [67] and a mass of 175 kg, including the safety casing, is adopted.

Another feature is the piezoelectric de-icing system. Small piezoelectric actuators are mounted on the inside of the leading-edge wall, exerting impulses and shear forces. Venna et al. [64] estimates 95% less energy consumption and 93% mass savings compared to existing electrical deicing systems.

Based on the engine geometry and on the densities of the applied materials, GasTurb© calculates the engine mass. This was verified with empirical formulas with factors for the advanced materials which were calibrated with data from the JT8D engine. The materials used are ceramic matrix composites (CMC) in hot parts and carbon fiber reinforced polymers, 3D waved for the three fan stages and with other manufacturing methods in parts of the casing. The rotating parts of the front part of the compressor consist of titanium whereas the last three are made of titan-alumides due to the higher thermal loads.

4.3.2 Stability

At the transition from subsonic to supersonic flight the aerodynamic center (AC) tends to move backwards which increases the longitudinal stability being defined as the distance between the center of gravity (CG) and aerodynamic center, related to the mean aerodynamic chord (MAC). How far and abrupt this occurs depends on the wing planform. For example, the backward shift of the AC of a highly swept wing or a delta wing is lower and less suddenly than for a low-sweep wing planform. [71]

Increasing the longitudinal stability means that if the aircraft is sufficiently stable in subsonic flight the trim drag will rise in supersonic flight. To counteract this problem there are several possibilities.

The first option, mostly applied at supersonic fighter aircraft, is the neutral stable or instable flying in the subsonic regime, which is possible with modern fly-by-wire flight controls but not allowed in commercial aircraft.

Another possibility is the controlled fuel consumption out of different tanks and the active tank to tank fuel transfer as adopted by the Concorde. This increases the development effort as well as the fuel system complexity and mass.

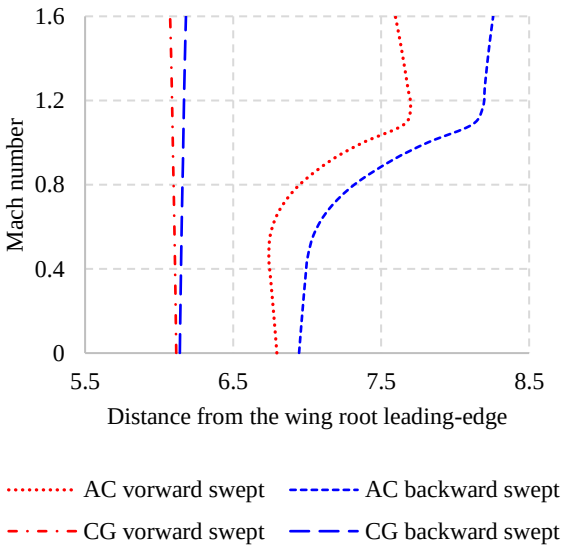

Figure 22. Aerodynamic center and center of gravity for variable forward and backward swept wings

The last presented opportunity is the forward variable-sweep wing. By sweeping the wing forward, on the one hand, the CG is shifted forward which increases the trim drag but on the other hand, the backward movement of the AC can be counteracted by sweeping the whole wing forward. For a variable backward swept wing, this works the other way around, which makes it even worse in terms of trim drag. These correlations are shown in Figure 22 where the position of the AC and the CG are presented for a variable backward and forward swept wing. With this technique, it is possible to fly a mission with 18 passengers having a static stability margin between 9% and 19% of MAC. Considering all possible positions of the CG, a range of 8% up to 25% of MAC is achieved. This should be sufficient for the conceptual design phase and could be investigated in detail in future work.

4.4 Propulsion

4.4.1 The Engine

This aircraft is equipped with two engines on top of the rear part of the fuselage. The requirements are a maximum take-off thrust of 95kN and a cruise thrust of 34kN per engine. The typical design case of a supersonic engine is the beginning of the cruise; however, the thrust required in the transonic flight regime must be provided, because the available thrust is also dependent on the flight Mach-number. This is seen in Figure 23 where the ratio of the thrust at take-off and cruise condition is displayed against the bypass ratio for different Mach numbers according to Howe [72].

An already existing engine was not applied because there are no modern civil engines available suitable for this flight regime. Furthermore, the engine parameters can be optimized for the HELESA design. The calculation of the applied engine was conducted with the gas turbine performance program GasTurb© and led to the relevant data presented in Table 6 and Table 7.

Geometry

Because the wave drag is very sensitive to the cross-sectional distribution, the engines should be as small as possible. In high altitudes, long ranges and for engines with small bypass ratios, turbofans with a mixed exhaust gas stream are more efficient than with two separate nozzles.

A research conducted by the NASA [73] analyzed six different engines amongst which were a turbine bypass engine, a variable cycle engine and a mixed flow turbofan. The weight, performance, takeoff noise, cruse emissions and size were analyzed for two supersonic commercial aircraft designs with a cruise speed of Mach 2.4 and a range of 5,000nm. They concluded that the mixed flow turbofan is the engine of choice because of its low mass, the less complex maintenance and the present experience. This indicates why even at this more sophisticated condition of more speed and range, the additional complexity of for example the variable cycle engine would not pay off.

	Values at Take-off condition
Bypass ratio	2.5
Overall pressure ratio	40
Maximum take-off thrust	95kN
Specific thrust	395 m/s
Burner exit temperature	1,650 K

Table 6. General engine data

Hence, a two-spool mixed flow turbofan with axial compressors and turbines is applied. The choice of a three-spool turbofan would be worthwhile only for engines with a higher thrust level and longer range airplanes due to its weight penalty. The application of a gearbox between turbine and fan is not sensible because of the small bypass ratio.

The fan has three stages, because of the need of a high pressure-ratio in the bypass. It is driven by the low-pressure turbine with two stages. The high-pressure compressor with 10 stages is driven by the high-pressure turbine with one stage. Immediately after the low-pressure turbine a lobed nozzle is installed to mix the core and bypass stream. An important parameter for the mixing efficiency is the length of the mixing area. [74]

The convergent-divergent nozzle has a variable geometry because of the operation in different flight regimes, subsonic, transonic and supersonic. It is equipped with a spike, which is movable forward and backward to alter the nozzle areas. This type has aerodynamic advantages even at subsonic speeds where the exhaust flow decompresses smoothly around the spike. [75]

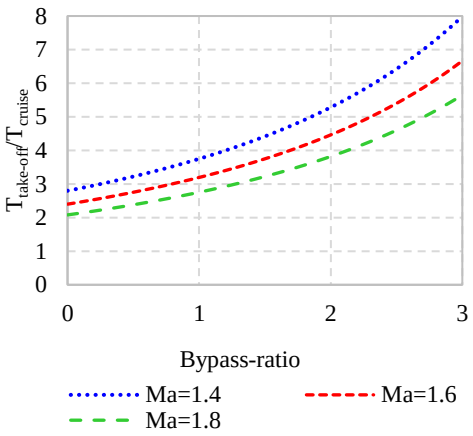

Figure 23. Thrust dependence from Mach-number and BPR

The landing distances and the acceleration-stop distance allows to avoid implementing a thrust reverser, saving weight, reducing complexity and ensuring quieter operations at airports.

As discussed in chapter 1, the engine efficiency, especially the thrust specific fuel consumption, has a direct influence on the total efficiency of the airplane.

Generally, there are two ways of improving the specific fuel consumption. Enhancing the propulsive and the thermal efficiency. [76]

Propulsive Efficiency

Improving the propulsive efficiency means lowering the relative exhaust speed while increasing the mass flow to maintain the same thrust level, thus increasing the bypass ratio. This can be seen in equation (4-2) wherein v_j is the jet velocity and v_0 the aircraft speed. [76]

$$\eta_{propulsion} = \frac{2}{1 + \frac{v_j}{v_0}} \tag{4-2}$$

Because a high exhaust velocity is needed and the engine must have a high specific thrust to keep the wave drag low, this is not the way of choice for increasing the total efficiency.

Another issue is the take-off noise which is especially for engines with small bypass ratios dominated by the exhaust jet noise. Eventually, the strong dependence of the thrust available in high altitudes on the bypass ratio, as seen in Figure 23, must be considered.

Nevertheless, a combined optimization with the aerodynamic efficiency of the whole airplane and the engine design parameters as well as the noise considerations would lead to the best compromise.

Thermal Efficiency

As a consequence, the focus is on the thermal or core efficiency. This is shown in equation (4-3) wherein π_c is the compressor pressure ratio, τ_0 the rise in total pressure due to the ram effect and κ the heat capacity ratio. [77]

$$\eta_{th} = 1 - \frac{1}{\tau_0 \cdot \pi_c^{\frac{\kappa-1}{\kappa}}} \tag{4-3}$$

That means the higher the pressure ratio and basically the Mach number, the better the thermal efficiency. This issue was approached by running several optimizations with GasTurb© having the goal to minimize the thrust specific fuel consumption. The most important parameters are the burner exit temperature, the bypass ratio, the inlet and mixer area and the pressure ratio of the inner and outer fan, the high-pressure compressor as well as the high and low-pressure turbine. The main constraints are the heat resistance of the applied materials, the inlet and mixer cross section area and the high-pressure compressor ratio. The latter determines the number of stages, the mass and length as well as the aerodynamic stability of the compressor and the ratio of the blade height to the gap between casing and blades of the last stages.

In order to improve the core efficiency advanced materials are implemented to avoid cooling air for the turbine and the combustor. Some other techniques are for example intercooling at the compressor, sequential combustion, recuperation or the constant-volume-combustion as well as their combinations. [78]

The sequential combustion neither increases the normalized thermal efficiency (with respect to the exergy) nor the core size, so it can be ruled out. The recuperation and the isochore combustion, for example realized with a wave-rotor, can just be implemented with an increase in the engine size, complexity and weight. Hence, the area of operation of these two possibilities are probably more in the subsonic regime. The most promising for supersonic engines is the intercooling

technologies. By cooling the air in the compressor, more mass flow can be realized which leads to a smaller core size. Furthermore, the cooling air for the turbine, bled off the compressor, has a lower temperature resulting in less cooling air and increased thermal efficiency. Nevertheless, the new materials approach was applied in order to avoid weight penalties and increased system complexity.

Mission segment	Specific Fuel consumption [lb/(h·lbf)]
Take-Off	0.49
Subsonic Climb	0.67
Subsonic Loiter	0.77
Subsonic Cruise	0.63
Transonic	0.74
Supersonic Climb	0.77
Supersonic Cruise	0.83
Supersonic Descent	0.74
Subsonic Descent	2.20

Table 7. Engine data for different segments

Special Features

The design is approached to the more electric aircraft principle resulting in no overboard bleed except at takeoff and landing where the internally blown flaps are used.

Ceramic matrix composites (CMC) are greatly applied in the hot segment of the engine, the combustor, the turbine and parts of the nozzle. Beside the weight saving there are other reasons concerning efficiency. The combustor is made of silicon-carbide fiber reinforced silicon-carbide ceramics (SiC-SiC) which has a high heat resistance up to 1,870K [65], so no cooling air is needed. This leads to less total burner pressure loss and consequently to a better combustor efficiency. Another advantage is the lower nitrogen oxide (NOx) emissions. NOx occurs at high temperature gradients or rather at high stoichiometric fuel rate gradients, which would be much less, if no cooling is necessary [79]. The same material (SiC-SiC) is applied in the turbine. This makes the cooling air unnecessary which has a big influence on the efficiency.

General Electrics is already using CMC´s in the new ADVENT engine in stationary and rotating parts. [80]

4.4.2 The Intake

The purposes of the intake are to convert the kinetic energy efficiently into static pressure at high speeds and to accelerate the flow at low speeds. [41]

Due to geometrical and structural reasons, an intake with a wedge is installed. According to Münzberg [76], at a Mach-number between 1.5 and 2.5 the outer supersonic compression is recommended. To minimize the total pressure loss, a three-shock intake was applied resulting in an intake total pressure-ratio of 0.99 without friction. [81]

Up to a Mach number of 1.7, there is no need for a variable intake without having high pressure losses which saves weight and complexity. [29]

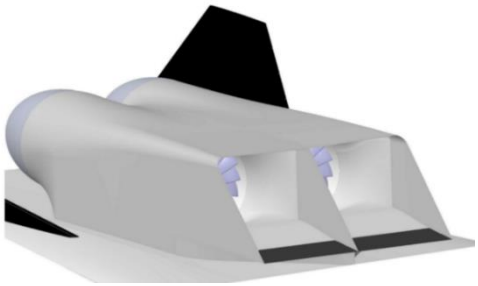

Figure 24. The intake

The geometry of the intake was developed according to Bräunling [77] and Anderson [82]. After the two oblique and the final perpendicular shock wave, the flow has a Mach number of 0.6 and before the fan after the subsonic diffusor the Mach-number is 0.55, which is in the recommended range of 0.4 to 0.7. [76]

The height of the boundary layer diverter was calculated according to Anderson [17] with the assumption of a turbulent boundary layer developing from the nose up to the intake.

4.4.3 Nitrogen Oxide Emissions

One of the HELESA design goals was the environmental consciousness of the aircraft, where the emissions, especially the NOx emissions are of vital importance.

The cruise NOx emissions are prescribed in the requirements to be comparable with current transonic transport aircraft. The value of comparison is the NOx emission index EI, which has the unit of grams of NOx per kg of fuel. Comparing several sources, an emission index for the current fleet of about 15 gNOx/kgFuel was assumed [83] [84] [85] [86]. Sun [12] defines an EI of 15 g/kg for aircraft below a cruise Mach number of 2 as sufficient.

According to Lefebvre [87], there are four types of NOx production, the thermal NOx, nitrous oxide mechanism, prompt NOx, and fuel NOx. To avoid the development of NOx, a lower combustor temperature, a lower pressure ratio, a homogeneous distribution of the fuel-to-air ratio and a short residence time is desirable [79] [87]. Unfortunately, a low combustor temperature and pressure ratio are generally speaking adverse to high thermodynamic efficiencies and a lower temperature as well as a shorter residence time results in high carbon monoxide (CO) and unburned hydrocarbons (UHC) emissions. Considering these effects, there exists a compromise of all emissions, which is approximately at combustor temperatures of between 1,680K and 1,900K [87]. This range is met by the designed engine for almost all mission segments.

Further possibilities to reduce the NOx emissions, based on conventional combustors, are for example the rich burn, quick quench and lean burnout principles, selective catalytic reduction or the exhaust gas recirculation. [88] [87]

Because the engine was calculated with GasTurb©, all values are available to calculate the NOx severity parameter S_{NO_x} and subsequently the NOx emission index [89] [90]. The used combustor is a combination of a Lean Premix Prevaporize (LPP) combustor with no cooling air resulting from the application of ceramic matrix composites (CMC). A LPP combustor can

be described in three sections. In the first one, the fuel is injected, vaporized, and mixed with air. The goal is to achieve entire evaporation and mixing before the combustion takes place. In the second zone, the flames are stabilized before they end up in the third zone, which can be compared with a conventional dilution zone. By having this premixed and evaporated combustion, which takes place near the flame blowout point, there is a uniform temperature pattern with very low NOx production. An important byproduct is, that almost no carbon is formed, which reduces not only emissions but also the heat transferred to the wall. This means less heat load for the material and vice versa a longer life time. Another advantage is, that under a temperature of 1,900K an increase in residence time does not lead to an increase of NOx formation [91] [92]. Hence, the residence time can be longer resulting in lower CO and UHC emissions. [87]

The two main problems are the autoignition, caused by the long mixing time, and the acoustics of the combustor. [87]

A study examined exactly the combination of the application of CMC's and a LPP combustion, resulted in an 80% reduction of the NOx emission index compared with conventional combustors. [93]

Applying these values, the NOx emission index for a conventional, a dual annular and a LPP combustor for the different flight segments is presented in Figure 25. It can be seen, that the NOx EI at subsonic cruise condition of the conventional combustor of 16 g/kg almost coincides with the average transonic fleet NOx EI of 15 g/kg. But looking at the supersonic cruise condition with a conventional combustor, the NOx EI would reach a value of 96 g/kg, which shows that new unconventional technologies are inevitable. The dual annular combustor results in cruise condition in a NOx EI of 69 g/kg, which would still be rather high. With a LPP combustor, the NOx EI with 19 g/kg at supersonic cruise conditions approaches the desired 15 g/kg, nevertheless, it is still too high. At least, with the LPP combustor the NOx EI of the flight segments covered by the LTO cycle by the ICAO [94], is achieved and compared with the subsonic flight condition of current subsonic engines, the NOx EI of 3.2 is much lower than the average one [95]. Furthermore, the emissions while taxiing are zero, thanks to the electrical ground taxi system (EGTS) reducing the pollution at airports and their surroundings.

As seen, even with new unconventional techniques, the target of a NOx EI of 15 g/kg in supersonic cruise condition is hard to achieve whereas the requirements of the LTO cycle are fulfilled and low subsonic cruise NOx EI values are attained.

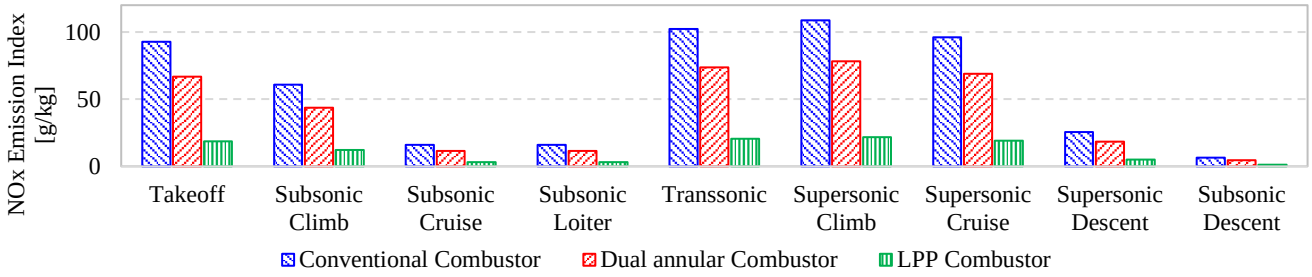

Figure 25. NOx emission index for different flight segments

4.5 Systems

4.5.1 High-Lift

There are two high-lift systems applied: an internally blown flap on the outer wing and an upper surface blown flap between the V-tail at the rear. The minimum sweep of the outer wing has been set to 20°, since a further reduction would increase the complexity and mass of the sweeping mechanism without improving the aerodynamics significantly.

The internally blown flaps have been implemented because of their high lift potential, their lower noise production especially during approach and the possibility to adapt the thin supersonic airfoils with the optimum camber in subsonic conditions.

The possible maximum lift coefficient without slats is 6 according to Radespiel [96]. Applying a safety margin, a maximum high lift coefficient for the airfoil of 4.5 is assumed. The required bleed air from the engines is calculated to 6 kg/s per engine according to Werner-Spatz et al. [97]. The high lift coefficient for the area with the externally blown flaps was estimated according to Dubs [98] to 1.35. This leads to a total maximum lift coefficient of 1.75 at landing conditions and 1.5 at the start.

The aerodynamics at take-off and landing as seen in form of a drag polar in Figure 37 in appendix J are calculated with analytical methods from Raymer [9] and Howe [72] as well as with the software xflr5 v6, with which the ring vortex method was used. The internal blown flaps are not contained in the known preliminary drag estimation methods, so assumptions had to be made which increases the deviation of the data and leaves space for further investigations.

Takeoff distances

The take-off distances were calculated according to Raymer [9]. The breaking coefficients, which are dependent on the velocity,

Elevation [m]	0		2500	
Runway condition	dry	wet	dry	wet
s_{TO} [m]	1,450	1,500	1,750	1,800
s_{TOEF} [m]	1,690	1,750	2,100	2,200
s_{AS} [m]	1,850	2,300	2,400	3,100
S_{TOFL} [m]	1,850	2,300	2,400	3,100

Table 8. Take-off distances

the tire pressure and the used anti-skid system are estimated with equations from the regulations CS-25 [6]. The take-off field length can be determined by the following equation (4-4).

$$s_{TOFL} = max\{1.15 \cdot s_{TO}\ ;\ s_{TOEF}\ ;\ s_{AS}\} \quad (4\text{-}4)$$

In Table 8 the take-off distances for different runway conditions and airport elevations are shown. For example, the Mexico City international airport with an elevation of 2,230m and a runway length of 3,900m lies far within the performance capability of the aircraft.

4.5.2 Landing Gear

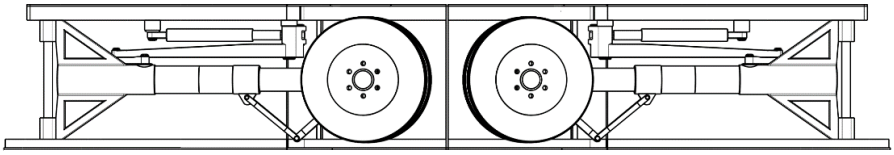

Figure 26. Landing gear mechanism

The landing gear location is in accordance with Raymer's standard recommendations [9]. The overturn angle should be less than 63° to ensure a secure landing with cross wind condition and sufficient stability on the ground while taxiing through corners. For the HELESA design, the overturn angle is 47°, as seen in Figure 38 in Appendix L. [9]

The landing gear must be long enough so that the tail does not hit the ground while landing with an angle of attack at 90% of the maximum lift condition minus the angle of incidence. As seen in Figure 27 the tail-down angle is 10° and thus higher than the angle of attack with 12.5° minus the angle of incidence with 3°. [9]

The wheel diameter and width as well as the oleo shock absorber length is calculated according to Raymer [9].

The wheelbase of 19.2m is slightly longer as that of the A321neo (16.9m [99]) but much less than for example a A350-900 (28.7m [100]). This indicates that there would be no issues with the standard taxiways.

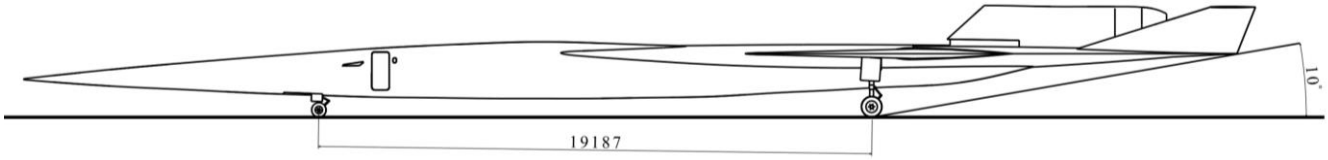

Figure 27. Landing gear position

4.5.3 Battery

Instead of an auxiliary power unit (APU), an advanced Lithium-Sulfur battery system with an energy density of 600Wh/kg [67] and a mass of 175kg, including the safety casing, is used.

With this battery, a turnaround of 1.8 hours, a 40 minutes taxi duration with the Electrical Ground Taxi System (EGTS) and several engine starts are possible.

The energy consumption on the ground is 30 kW without the electrical ground taxi system, calibrated with data from the Boeing 767-200ER. In cruise condition, the required electrical power is 150kW without considering the energy for recharging the battery, which was estimated according to data from the 787-8.

If the battery is emptied to the allowable level, it takes 1.5 hours of flight to fully recharge it. The use of a battery instead of the APU saves weight. The APU of the McDonnell Douglas MD-80 weighs 380kg [63] without considering the additional fuel and control system. Furthermore, it reduces the noise and emission at the airport and has a higher efficiency.

4.5.4 Electric Ground Taxi System

This aircraft is equipped with an Electric Ground Taxi System (EGTS) first developed by a joint venture of Honeywell and Safran [101] making a push back car superfluous. The ground taxi system consists of two electrical motors on each main landing gear which are powered by the battery. It is possible to taxi up to 40 minutes, which is even more than the longest average taxi time at the New York JFK Airport [102]. With the recovery of the energy due to breaking of 8.4%, an average power of 14.5kW is needed to taxi which results in 8.8kWh. [68]

With the EGTS the airport noise and the air pollution is minimized. The fuel savings for the whole mission is very hard to predict because of the highly dependence of the flown mission and the airports being served. According to Dzikus et al. [103], fuel savings of 1.1% up to 3.9% for the whole mission can be assumed considering also the additional weight. Because of the uncertainty of this values, 1% fuel saving is considered which should be a conservative estimation, especially for engines with a small bypass ratio and relatively high fuel consumptions while taxiing as used in the HELESA design.

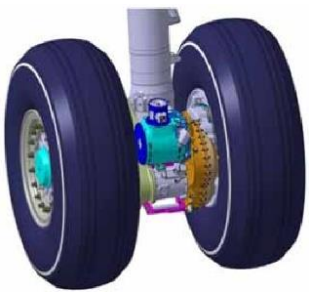

Figure 28. EGTS [151]

4.5.5 Flight Controls

The combined rudders and elevators are mounted at the V-tail and the ailerons at the outer wing. The pilot's inputs are transmitted electrically by the fly-by-wire (FBW) system that provides flexibility for the control laws for the supersonic and subsonic regime. Following the more electric aircraft approach an electrically power supply is adapted supporting the Electro-Hydrostatic (EHA) and Electro-Mechanical Actuators (EMA). Despite the reliability of the fly-by-wire system a mechanical backup is provided by an additional mechanical rudder and trim control inspired by the Airbus concept, allowing the aircraft to be operated also without the fly-by-wire computer. [104] [105]

4.6 Noise

4.6.1 ICAO Noise Regulations

Noise pollution near airports is a huge problem in aviation. Many different sources such as engine, landing gear or slats and flaps are responsible for noise generation. In 2013, the new ICAO standard, Chapter 14, was introduced whose guidelines are built on the Effective Perceived Noise level (EPNdB). Noise is measured at three reference points:

- → Fly-over: 6.5km from the brake release point, under the take-off flight path (Point 1)
- → Sideline: the highest noise measurement recorded at any point 450m from the runway axis during take-off (Point 2)
- → Approach: 2km from the runway threshold, under the approach flight path (Point 3)

As a rough guideline, the cumulative level, defined as the arithmetic sum of the certification levels at each of the three points, has to be 7 EPNdB below the chapter 4 regulated aircraft. [106]

Due to the difficulties of spatial noise calculations, in this study the determined values are based on approaches made by comparisons with an aircraft and engines in similar size and thrust class. For this, the McDonnell Douglas MD-81 with two JT8D-219 engines, which is listed under the regulations of chapter 4, was chosen. Although the aircraft is heavier than the HELESA design, the engines are in the same thrust class, which provides good comparable data.

	McDonnell Douglas MD-81 [EPNdB]	HELESA [EPNdB]	Percentage reduction [%]
Fly-over	85.3	81.0	5.0
Sideline	95.5	88.8	7.0
Approach	93.3	85.8	7.0
Cumulative	274.1	255.3	7.36
Cum. limit	286.8	267.0	7.40

Table 9. Noise levels of the HELESA design and comparable aircraft at airport reference points.

The result at the three reference points of the evaluation of 14 measurements with an average rating [107], are shown in Table 9.

Therefore, by taking the different weight class into account, the cumulative noise limit for this design is coarsely set to 267 EPNdB.

Since two engines are installed, each with a maximum take-off thrust of 95 kN and a small bypass ratio, consequently the jet exit velocity reaches high orders of magnitude making the jet noise the greatest shareholder of noise emission during take-off. Taking into account new applied technologies in comparison to the McDonnell Douglas MD-81, it is possible to reduce jet noise as well as noise emissions generated by the landing gear and the high-lift system, presented in Table 9.

According to Fishbach et al. [108], increasing the engines bypass ratio from 1.74 (JT8D-219) to 2.5 leads to a reduction of noise emission at all reference points, mainly at the sideline and fly-over point. Therefore, a reduction of 2% each at point 1 and 2 and a reduction of 1% at point 3 is assumed. Additionally, positioning the engine on top of the aircraft allows a shielding by the V-tail and the fuselage to the side and downwards [109]. For the noise shielding a decrease of 3% at point 1, 3% at point 2 and 2% at point 3 is expected. Investigations by Li et al. [110] using fairings, Pott-Polenske [111] and You et al. [112] using splitter plates at landing gears, leading to an audible reduction of noise emission in the far field, assumed with 1% at point 2 and 2% at point 3. With the partial installation of internally blown

	$\Delta p_{max}\ [Pa]$	$\Delta t\ [ms]$	$rise\ time\ [ms]$	$[PLdB]$
Cruise begin	41.4	77.3	8.5	86
Cruise end	28.1	77.1	8.5	81
Climb supersonic	38.7	60.5	6.7	87
Descent supersonic	41.2	56.8	6.2	85

Table 10. Maximum pressure differences, duration of pressure disturbance, the rise time of the first pressure peak and the loudness level for different mission segments

flaps replacing conventional high-lift systems, especially noise emission during approach decreases which results in a reduction of 1% at point 2 and 3% at point 3.

In total, an overall noise reduction for fly-over of 5% and 7% for the sideline and the approach reference point compared with the calibrated values from the MD-81 is reached. With these assumptions, the compliance of the new ICAO standard, Chapter 14, is achieved.

4.6.2 Sonic Boom

The low boom design aspect was not considered in the HELESA design because of the negative influence on the fuel-efficiency. Nevertheless, the sonic boom was estimated to get an impression of the noise level.

Every projectile causes a pressure signature during supersonic flight, which can be defined in a near, mid and far-field pressure signature. [113]

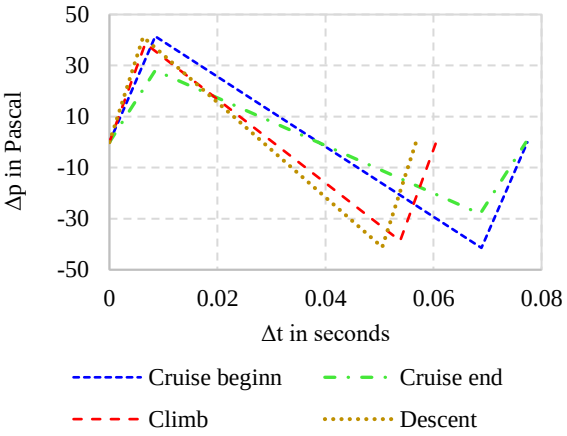

Figure 29. Far-field pressure signatures for different mission segments

Whitham [114] was one of the first scientists to develop a mathematical theory for calculating the disturbance in the air of a projectile with supersonic speed. He introduces the F-function seen in equation (4-5) which is obtained by the second derivation of the equivalent body distribution A'' due to volume and lift. Compared with the infinite equivalent bodies for every bank angle obtained for the wave-drag calculation, just one area and lift distribution is needed because the sonic boom below and not above or next to the airplane is of interest.

To calculate the far field pressure signature, the method from Carlson [115] is applied. The atmosphere, the bank and the climb angle influences the pressure formation while propagating towards the ground. Four different flight conditions are calculated without any bank angle and with simple assumptions for the atmosphere. In Table 10, the results for the different mission segments are presented.

$$F(x) = \frac{1}{2\pi}\int_0^x \frac{A''}{\sqrt{x-t}}\,dt \qquad (4\text{-}5)$$

To convert the pressure signatures of the different mission segments into a loudness level (phone) the method of May [116] was used. Beside the shape of the pressure distribution itself, the rise time and the first maximum overpressure are the two main parameters to influence the noise level.

The loudness level (phone) is converted into loudness (sone) [117] and subsequently into a perceived noise level (PLdB) according to Stevens [118].

The difference between the loudness level of climb and descent conditions arise because of the different ray path lengths resulting from the different flight path angle. In climb conditions, the ray path is about 12.5 km whereas it is just 11km in the descent condition.

The width of the audible boom on the ground is about 30nm [119].

With greater focus on the low boom design aspects, concerning for example a higher wing dihedral angle or the adaption of the equivalent areas to get a more convenient ground pressure signature, there is potential to reach the 75PLdB with some negative effects on fuel efficiency.

In Table 12 in appendix K, some possibilities of obtaining a lower perceived noise level are listed with an assessment for the applicability to the HELESA design and the estimated influence on the efficiency in terms of fuel consumption. A promising possibility could be the retractable front spike [120]. It has a noticeable influence at the perceived noise level with just minor disadvantages in structural weight. It is extended in supersonic flight condition to produce, instead of one big nose shock, several little ones, resulting from different spike cross section areas. The challenge is the right pattern of the distance as well as the strength of each little shock, to avoid their combination to one big shock wave, on the way towards the ground.

In future work, the low boom aspect could be analyzed in order to achieve the required 75dB.

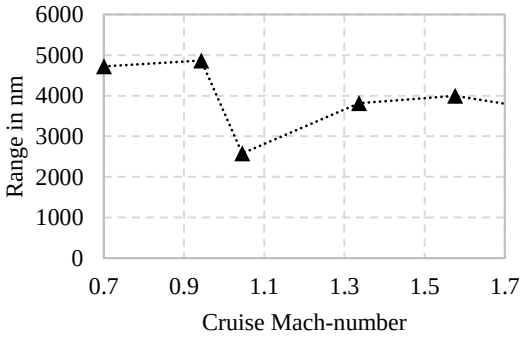

Figure 30. Possible maximum range for different cruising speeds

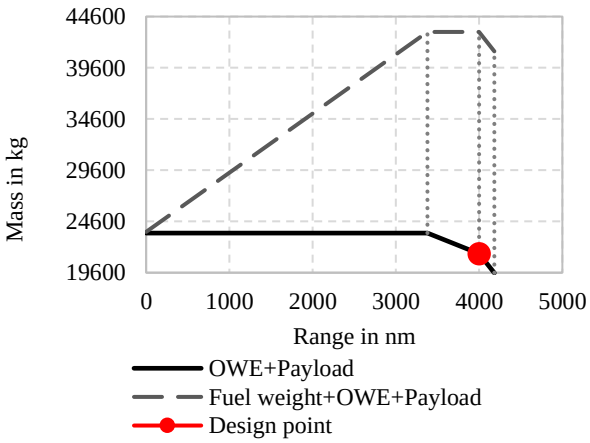

Figure 31. Payload-Range diagram

4.7 The Mission

4.7.1 Possible Missions

Flying at supersonic speeds over ground is not allowed in the U.S. (FAR Part 91.817) whereas in Germany and many other countries, the sonic boom must not reach the ground (LuftVO Section 11). That means the aircraft can fly at cruise altitude and in normal atmospheric condition up to the cutoff Mach number. This Mach number is estimated according to Lindsay and Maglieri [121] for zero climb angle and for the critical case of a cold day of standard atmosphere minus 22°C (-40°F) to Mach 1.12. However, flying at this Mach number is very inefficient due to the high wave drag in this transonic regime, as seen in Figure 30. In Figure 32 and Figure 33 the possible ranges and the needed flying time is presented for different supersonic to transonic and supersonic to subsonic fractions. The payload range diagram in Figure 31 is calculated for cruise entirerly at Mach 1.6, beside the climb and descent phases. The design payload is calculated to 1,890kg by assuming an average passenger mass of 85kg with a baggage mass of 20kg. The maximum Payload ist defined to 3,890kg. In Figure 31, the high fuel fraction is clearly visible.

Another payload-range diagram is shown in Appendix N in dependency of the cruise Mach number. Ranges for different Mach numbers and payload is listet in Table 11. The visualization of different missions is presented in Appendix P.

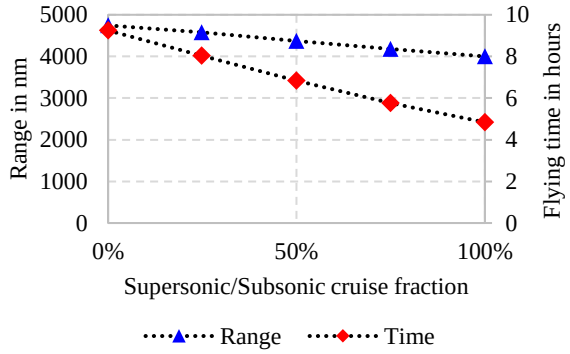

Figure 32. Range and time for different super/trans cruise fractions

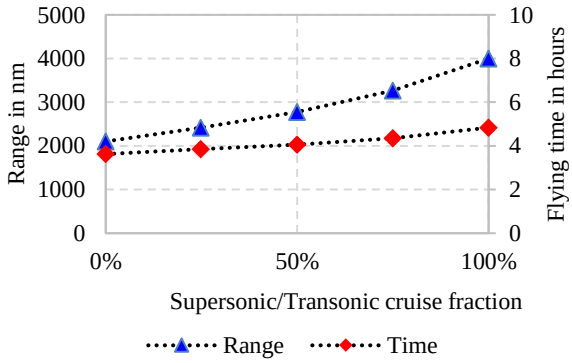

Figure 33. Range and time for different super/sub cruise fractions

4.7.2 Maximum Cruise Altitude

While defining the maximum cruise altitude, the following aspects are considered.

One problem of flying at high altitudes are the emissions and their impact on the atmosphere. By considering the study conducted by NASA [122], investigating the impact of a supersonic business jet fleet on the atmosphere, Sun et al. [12] recommends a maximum altitude of 17km in terms of ozone depletion. The cosmic radiation, being dependent on the "altitude, the geomagnetic latitude and the solar cycle" [123], must be considered too. The International Commission on Radiological Protection proposes a maximum dose of 20 millisievert (mSv) per year, averaged in 5 years and with no one year average higher than 50mSv. The results from a recent study made by Bagshaw [123], examining the present air travel, were 2-3mSv per year for long-haul and 1-2mSv per year for short-haul pilots. The Concorde, which had a cruise altitude of 18.3km had a radiation meter on board which could be read at the flight engineer panel. In 1979, a solar active year, the average data showed 2.75mSv per year for the technical crew and 2.19mSv per year for the cabin crew [124]. Hence, with a maximum altitude of 17km, radiation should not be an issue. The last point to be considered is the pressurization. The regulations for large airplanes CS 25.841 [6] specifies, if certificated for more than 7,620m, a cabin pressure of no more than 4,572m must be maintained at any probable failure.

Looking at these three considerations the maximum altitude is limited to 17km.

4.7.3 Ground Operation

The feasibility and reliability of a fast turnaround is of vital importance for everyday use in service.

While the plane is on the apron, the wings are in the supersonic position therefore reducing the possibility of impacting with airport vehicles or infrastructure while also requiring less space at the parking position. The baggage, passengers and fuel can be handled simultaneously because different spatially separated accesses are available.

Cruise Mach number	Payload in kg	Range in nm
1.6	1,890	4,000
1.6	0	4,183
1.6	3,890	3,376
1.1	1,890	2,102
1.1	0	2,177
1.1	3,890	1,769
0.92	1,890	4,746
0.92	0	4,926
0.92	3,890	3,962

Table 11. Ranges for different Mach numbers and payload

4.8 Concluding Studies

The Feasibility

The applied new technologies are discussed with respect to their feasibility, starting with the wing. Since the aerodynamic performance of the forward variable-sweep wing was assumed to be the same as for a backwards swept, except the advantage of the aerodynamic center shift counteraction, the reliability should be acceptable. The adapted technique to realize a 40% laminar flow portion on the upper wing in the supersonic flight regime was tested by the JAXA with an unmanned scaled test plane showing good performance. Much development effort would be required to consider the fact that a special pressure signature for the supersonic laminar flow technologies should be obtained at the same time without diminishing the aerodynamic efficiency in other flight regimes.

The variable-sweep mechanism results in higher complexity and maintenance but is a well-known technology in the military sector. Differently the high lift system has only been investigated in theory and has never been implemented before.

Regarding the structural design, constructing many parts with fiber reinforced materials is a known technology meanwhile, considering the A350, the B787 or some newcomer such as the Irkut MC-21 or the Bombardier CSeries. Nevertheless, uncertainties exist on the one hand by constructing almost all structural elements with fiber reinforced polymers and on the other hand by considering the customer acceptance of a fuselage with almost no windows.

The application of ceramic matrix composites in stationary and rotary parts of the engine should be feasible, considering that General Electrics uses this material in operating engines. The lean premix prevaporized combustor has probably the highest risk. However, its implementation would not affect the aircraft performance directly while significantly improving emissions, especially at high altitudes. Specifically, in the HELESA design goal of constructing an environmental acceptable aircraft.

Proceeding with the battery, uncertainties result in the assumed energy density, adapted from the new battery generation. The EGTS is an already tested and known technology which is very likely to become a standard feature of next generation transport aircraft.

Looking at all these technologies, highest risks result from the high lift system for the outer wing and the new combustor. Assuming the case of applying a conventional combustor and a double slotted flap, the wing area, the approach noise level and the emissions would increase, resulting in lower overall efficiency but nevertheless, this concept would still reach sufficient performance characteristics.

All in all, a conservative design philosophy has been followed throughout this project, so that this concept would be able to tolerate a drawback in the riskiest applied technologies.

Cost and Market

Providing a thorough analysis regarding cost estimation of an airplane in conceptual design is extremely difficult since information such as a complete program plan, labor and material analysis or subcontractor inputs are unavailable. At this early stage, the approach is to rely on statistical methods as well as on cost comparisons with similar aircraft configurations. But even comparing similar aircraft is challenging especially between new and old configurations or between newly designed and evolved aircraft having already underwent the „learning-curve effect" [9]. Furthermore, the access to detailed costs is often limited.

To make concrete predictions, the whole life-cycle costs should be taken into account. This can be divided into the costs for research, development, test and evaluation (RDT&E), production, ground support and equipment, initial spares and operations and maintenance.

For the estimation of the costs the modified "DAPCA IV Model (2012) – Development and Procurement Costs of Aircraft model" was employed. It has been developed by the RAND Corporation, [125] [126]. Table 13 in Appendix O outlines the results for the different areas. In view of the fact that the company "Boom" reached 76 orders at the 2017 International Paris air show for their supersonic transport aircraft, a total production of 100 aircraft is assumed [127]. The result of a total cost of $107.5 million for one aircraft and operation costs of $49,177 per flight seem to be reasonable compared to the costs for the SSBJ's of Aerion ($80 million), Dassault ($83 million) [128] and Boom ($200 million) [127].

Discussion of former and current Configurations and Concept Designs

A comparison of this aircraft with other configurations is described in this section in order to assess the performance in relation to contemporary and former designs. Data are presented in appendix Q in Table 14. The Aérospatiale - BAC Concorde and the Tupolev Tu-144 are not convenient for comparison, since they were much larger and heavier. Hence designs which have their entry into service at the mid 2020's will be considered.

The already mentioned AS2 from Aerion Cooperation with its supersonic low sweep natural laminar flow wing is one of the most advanced designs. With a cruise speed of Mach 1.4 it is more suitable in terms of comparison. With a capacity of up to 10 passengers, it has a maximum range at supersonic speed of 4,750nm, a MTOM of 54,884kg and a takeoff thrust of 3 x 71-75kN. Comparing the HELESA design with the AS2, having 8 passengers less, a lower cruise speed and 750nm more range, it is almost 12,000kg heavier and needs approximately 40kN more thrust. This means, assuming all data are comparable, that the current design with its new applications, especially the different wing type, is more efficient.

Another interesting design is the Spike S-512. Their first design consisted of the low sweep natural laminar flow wing, which was later changed to a delta wing instead [12]. This design has the same cruise Mach number and the same maximum capacity of 18 passenger. At a range of 5,580nm this plane has a MTOM of 52,163kg and a maximum takeoff thrust of 2 x 88.9kN. So, with a 1,580nm longer range it is about 9,000kg heavier than the HELESA design.

It is important to mention that the range for the S-512 at supersonic speed is 1,500nm higher than for cruise at subsonic speeds whereas in the HELESA design, the subsonic range is 750nm longer resulting in more flexibility.

In the course of the European research project HIghSpeed AirCraft (HISAC), three aircraft were designed with different objectives having pretty much the same requirements as the current design. The aircraft with the low take-off noise objective having been design by Dassault has a MTOM of 51,100kg with a maximum take-off thrust of 220kN for 8 passengers.

The last design being discussed is the SAI Quiet Supersonic Transport aircraft. With the same cruise Mach number, range and a capacity of 12-16 passengers, this design is almost 17,000kg heavier and needs approximately 100kN more takeoff thrust than the present one. This significant difference could be caused, amongst others, by the strong focus on the low boom design aspect.

The comparison of the current fuel consumption of 6.6 pkm/kg with that of a Gulfstream G650 with 9.7 pkm/kg, calculated with data presented in Aviation Week [129] shows, that the HELESA designed aircraft has a 32% higher fuel consumption for a 78% faster cruise speed.

5 Conclusion

In this project a supersonic business class aircraft with a cruise Mach number of 1.6, a range of 4,000nm and a capacity of 18 passenger has been developed. The design tools range from analytical methods to advanced software programs.

The requirements are a cruise Mach number of 1.6 to 1.8, a design range of 4,000nm, a payload of 6 to 20 passenger, a fuel efficiency of at least 3.55 Passenger-kilometre per kilograms of fuel (pkm/kg) for a supersonic mission and a take-off field length less than 2,133m.

The main design goal was the environmental acceptability of this aircraft resulting in additional requirements such as a supersonic cruise NOx emission index comparable to current transonic aircraft and airport noise according to ICAO chapter 14.

In order to achieve this, the low boom aspect was neglected because of the inherent contradiction between low-boom and high-efficiency designs.

To cope with the efficiency objectives, the High-Efficient Low-Emission Supersonic Aircraft (HELESA) design has been focused on the aerodynamic efficiency in both subsonic and supersonic flight, the minimization of structural weight fraction and of the engine specific fuel consumptions.

The results in terms of environmental compatibility are a fuel efficiency of 6.6 pkm/kg, a cruise emission index of 19 grams of NOx per kg of fuel (g/kg) and a cumulative Effective Perceived Noise level (EPNdB) of 267dB.

Judging these results, the fuel efficiency is almost twice as good as prescribed and the EPNdB is in compliance with Chapter 14 whereas the NOx emission index is slightly higher than prescribed. Nevertheless, the emissions for the landing and take-off cycle (LTO) described by the ICAO as well as in the subsonic cruise condition is far within the bounds.

Despite the impossibility of supersonic flight over land, routes that are not entirely over water can be operated in a fast and efficient way due to the high aerodynamic efficiency in the subsonic regime, providing great operational flexibility. Hence routes such as Europe to the East Coast of the USA would be a very attractive business case for the HELESA design.

The results show the potential of a forward-swept, variable-sweep wing, combined with advanced engine technologies as well as improvements in systems and structural design.

Further studies could include an advanced wing design considering the special pressure distributions in supersonic flight for the laminar flow, a more sophisticated wave drag optimization as well as the improvement of the empirical mass estimation methods. Tests could be conducted considering the optimization of the aerodynamic center movement counteraction by the variable forward-swept wing arising while the transition from subsonic through transonic to supersonic flight regimes.

6 Acknowledgment

Special thanks go to M. Rizzato and Prof. A. Strohmayer for their constant support and availability to help with all the questions and for the close guidance provided.

Recognition also goes to Dr. O. Brodersen, Dr. K. Pahlke and F. Dambowski of DLR for all the planning and coordination of this Design Challenge making it possible in the first place.

List of References

[1] B. Liebhardt and K. Lütjens , "An Analysis of the Market Environment for Supersonic Business Jets," German Aerospace Center (DLR) – Air Transportation Systems, Hamburg , 2011.

[2] S. Horinouchi, "Conceptual Design of a Low Sonic Boom SSBJ," AIAA, 43rd AIAA Aerospace Sciences Meeting and Exhibit , Reno, Nevada, 2005.

[3] J. A. Rosero, J. A. Ortega, E. Aldabas and L. Romeral, "Moving Towards a More Electric Aircraft," IEEE A&E SYSTEMS MAGAZINE,, 2007.

[4] A. Strohmayer, *Flugzeugentwurf I, Foliensatz,* Universität Stuttgart: Institut für Flugzeugbau, 2015.

[5] International Civil Aviation Organisation, Aircraft Operations, Volume I, Flight Procedures, 5 ed., 2006.

[6] European Aviation Safety Agency, Certification Specifications and Acceptable Means of Compliance for Large Aeroplanes, CS-25, Amendment 18, 2016.

[7] Bombardier, "Business Aircraft," 2016. [Online]. Available: http://www.businessaircraft.bombardier.com/en/aircraft. [Accessed 06 Juni 2017].

[8] Cessna, "Textron Aviation," 2017. [Online]. Available: http://cessna.txtav.com/en. [Accessed 06 Juni 2017].

[9] D. P. Raymer, Aircraft design, A Conceptual Approach, 5 ed., Reston, Virginia: American Institute of Aeronautics and Astronautics, 2012.

[10] P. M. Hartwich, B. A. Burroughs, J. S. Herzberg and C. D. Wiler, "Design development strategies and technology Integration for supersonic Aircraft of low preceived Sonic Boom," The Boeing Company – Phantom Works , Huntington Beach, USA, 2003.

[11] Spike Aerospace, Inc., 2013-2017 . [Online]. Available: http://www.spikeaerospace.com/s-512-supersonic-jet/multiplex-digital-cabin/. [Accessed 15 June 2017].

[12] Y. Sun and H. Smith, "Review and prospect of supersonic business jet design," Progress in Aerospace Sciences, 2016.

[13] R. Whitford, Design for Air Combat, London: Jane's Publishing Inc., 1987.

[14] T. Lutz, Skript zur Vorlesung "Flugzeugaerodynamik I & II", Stuttgart: Institute of Aerodynamics and Gas dynamics (IAG), 2013.

[15] A. G. Panaras , Aerodynamic Principles of Flight Vehicles, Reston, Virginia: American Institute of Aeronautics and Astronautics, 2012.

[16] E. Torenbeek, E. Jesse and M. Laban, "Conceptual Design and Analysis of a Mach 1.6 Airliner," American Institute of Aeronautics and Astronautics, Albany, New York, 2004.

[17] J. D. Anderson, Jr., Fundamentals of Aerodynamics, 5 ed., New York: McGraw-Hill Series in Aeronautical and Aerospace Engineering, 2011.

[18] F. M. White, Viscous Fluid Flow, New York: McGraw-Hill, 1991.

[19] L. M. Mack, "Linear Stability Theory and the Problem of Supersonic Boundary-Layer Transition," Jet Propulsion Laboratory, Pasadena, California, 1975.

[20] P. Sturdza , An aerodynamic Design Method for supersonic natural laminar Flow Aircraft, Department of aeronautics and astronautics and the committee on graduate studies of stanford university : Peter Sturdza, 2004.

[21] R. R. Tracy, "High Efficiency, Sipersonic Aircraft". United States Patent 5,322,242, 21 Jun 1994.

[22] J. G. McTigue, J. D. Overton and G. J. Petty, "Two Techniques for Detecting Boundary-Layer Transition in Flight at Supersonic Speeds and at Altitudes Above 20,000 Feet," National Aeronautics and Space Administration, Washington, 1959.

[23] D. W. Banks, C. P. van Dam , H. J. Shiu and G. M. Miller, "Visualization of In-Flight Flow Phenomena," National Aeronautics and, Dryden Flight Research Center Edwards, California, 2000.

[24] AERION Corporation, "AerionSupersonic," 2017. [Online]. Available: http://www.aerionsupersonic.com/. [Accessed 10 Jun 2017].

[25] T. Ohnuki, K. Hirako and K. Sakata , National Experimental Supersonic Transport Project, Japan: Japan Aerospace Exploration Agency, 2006.

[26] H. Schlichting and K. Gersten, Grenzschicht-Theorie, 10 ed., Berlin, Heidelberg: Springer-Verlag, 2006.

[27] K. Yoshida, "Supersonic drag reduction technology in the scaled supersonic experimental airplane project by JAXA," Progress in Aerospace Sciences, Tokyo, Japan, 2009.

[28] W. S. Saric and H. L. Reed, "Supersonic Laminar Flow Control on Sewpt Wings Using Distributed Roughness," 40th Aerospace Sciences Meeting & Exhibit, Reno, Nevada, 2002 .

[29] M. Schuermann, Supersonic Business Jets in Preliminary Aircraft Design, Braunschweig: TU Braunschweig Institut für Flugzeugbau und Leichtbau , 2016.

[30] T. von Karman, "The problem of resistance in compressible fluids," Atti del V Convegno della "Fondazione Alessandro Volta," , Rome, 1935.

[31] W. Haack, "Geschossformen kleinsten Wellenwiderstandes,," Bericht 139 der Lilienthal-Gesellschaft fur Luftfahrt, 1941.

[32] W. R. Sears, "On Projectiles of minimum Wave Drag," Quarterly of Applied Mathematics, Cornell University, 1947.

[33] R. T. Whitcomb, "A Study of the Zero-Lift Drag-Rise Characteristics of Wing-Body Combinations Near the Speed of Sound," NACA Report 1273, Langley Field, VA, United States, 1952.

[34] R. T. Jones, "Theory of Wing-Body Drag at Supersonic Speeds," NACA Technical Report 1284., Moffett Field, CA, United States, 1953.

[35] H. Lomax, "The Wave Drag of Arbitrary Configurations in Linearized Flow As Determined by Areas and Forces in Oblique Planes," National Advisory Committee for Aeronautics, Washington, 1955.

[36] R. V. Harris, Jr., "An Analysis and Correlation of Aircraft Wave Drag," NASA, Washington, D.C., 1964.

[37] L. A. McCullers, "AWAVE: User's guide for the revised wave drag analysis program," NASA Langley Research Center, 1992.

[38] M. J. Waddington, "Development of an interactive Drag Capability for the OpenVSP parametric Geometry Tool," Faculty of California Polytechnic State University, San Luis Obispo, 2015.

[39] E. Eminton and T. Lord, "Note on the Numerical Evaluation of the Wave Drag of Smooth Slender Bodies Using Optimum Area Distributions for Minimum Wave Drag," Journal of the Royal Aeronautical Society 60, Cambridge University, 1956.

[40] F. Dubs, Hochgeschwindigkeits-Aerodynamik, Basel: Springer Basel AG, 1975.

[41] E. Krämer, "Kampfflugzeuge," in *Handbuch der Luftfahrzeugtechnik*, C. Rossow, K. Wolf and H. Peter, Eds., München, Carl Hanser Fachbuchverlag, 2014, pp. 113 - 150.

[42] P. Sturdza, "Extensive Supersonic Natural Laminar Flow on the Aerion Business Jet," 45th AIAA Aerospace Sciences Meeting and Exhibit, Reno, Nevada, 2007.

[43] B. Adolf, "Aerodynamic lift at supersonic speeds," Luftfahrtforschung, Rome, 1935.

[44] W. H. Liepmann and A. Roshko, "Elements of Gas Dynamics," John Wiley & Sons, Inc., New York, 1957.

[45] K. Kusunose, K. Matsushima, Y. Goto, H. Yamashita, M. Yonezawa, D. Maruyama and T. Nakano, "A Fundamental Study for the Development of Boomless Supersonic Transport Aircraft," 44th AIAA Aerospace Sciences Meeting and Exhibit , Reno, Nevada, 2006.

[46] K. Kusunose, K. Matsushima and D. Maruyama, "Supersonic biplane-A review," Progress in Aerospace Sciences, 2010.

[47] M. R. Licher, "Optimum Two-Dimensional Multiplanes in Supersonic Flow," Douglass Aircraft Company, 1955.

[48] K. Kusunose , K. Matsushima , S. Obayashi , T. Furukawa , N. Kuratani , Y. Goto and et al., "Aerodynamic design of supersonic biplane: cutting edge and related topics," Tohoku University Press, Japan, 2007.

[49] D. M. Van Wie, F. T. Kwok and R. F. Walsh, "Starting characteristics of supersonic inlets," American Institute of Aeronautics and Astronautics, Inc., Lake Buena Vista, 1996.

[50] H. Yamashita, M. Yonezawa and S. Obayashi, "A Study of Busemann-type Biplane for Avoiding Choked Flow," American Institute of Aeronautics and Astronautics , 2007.

[51] D. Maruyama, K. Matsushima, K. Kusunose and K. Nakahashi, "Aerodynamic Design of Biplane Airfoils for Low Wave Drag Supersonic Flight," 24th Applied Aerodynamics Conference, San Francisco, California, 2006.

[52] D. Maruyama, T. Matsuzawa, K. Kusunose, K. Matsushima and K. Nakahashi, "Consideration at Off-design Conditions of Supersonic Flows around Biplane Airfoils," 45th AIAA Aerospace Sciences Meeting and Exhibit , Reno, Nevada, 2007.

[53] M. Moore and D. Frei, "X-29 Forward Swept Wing Aerodynamic Overview," AlAA Applied Aerodynamics Conference , Danvers, Massachusetts , 1983.

[54] E. J. Saltzman and J. W. Hicks , "In-Flight Lift-Drag Characteristics for a Forward-Swept Wing Aircraft (and Comparisions With Contemporary Aircraft)," National Aeronautics and Space Administration, Washington, DC, 1994.

[55] P. Purser and J. Campbell, "Experimental Verification of a Simplified VeeTail Theory and Analysis of Available Data on Complete Models with Vee Tails," NACA 823, 1945.

[56] A. Ferri, "Elements of aerodynamics of supersonic flows," The Macmillan Company, New York, 1949.

[57] A. Ferri, "Experiments at supersonic speed on a biplane of the Busemann type," Ministry of Aircraft Production, 1944.

[58] T. Furukawa , N. Kumagai , S. Oshiba , T. Ogawa , K. Saito and A. Sasoh , " Measurement of pressure field near Busemann's biplane in supersonic flow," Proceedings of the annual meeting and the seventh symposium on propulsion system for reusable launch vehicles, Northern Section of the Japan Society for Aeronautical and Space Sciences, vol. G-17, 2006.

[59] H. A. A. Gerhardt, "Lifting Shock Wave Cancelation Module". United States Patent 4,582,276 , 15 April 1986.

[60] H. Schlichting and E. Truckenbrodt, Aerodynamik des Flugzeuges, vol. I, Berlin/Göttingen/Heidelberg: Springer Verlag, 1959.

[61] A. Higgins, "Adhesive bonding of aircraft structures," International Journal of Adhesion & Adhesives , 2000.

[62] E. Torenbeek, Synthesis of subsonic airplane design, Rotterdam: Delft University Press , 1976 .

[63] J. Roskam, Part V: Component weight estimation, Ottawa, Kansas: Roskam Aviation and Engineering Corporation, 1985.

[64] S. V. Venna, Y.-J. Lin and B. Galdemir, "Piezoelectric Transducer Actuated Leading Edge De-Icing with Simultaneous Shear and Impulse Force," Journal of Aircraft, University of Akron, Akron, Ohio, 2007.

[65] F. Raether , "Ceramic Matrix Composites - an Alternative for Challenging Construction Tasks," Fraunhofer Center for High Temperature Materials and Design HTL, Bayreuth, Germany, 2013.

[66] K.-H. Grote and J. Feldhusen, Dubbel, Taschenbuch für den Maschinenbau, 22 ed., Berlin Heidelberg: Springer, 2007.

[67] A. Manthiram, Y. Fu and Y.-S. Su, "Challenges and Prospects of Lithium-Sulfur Batteries," Accounts of Chemical Research, Electrochemical Energy Laboratory & Materials Science and Engineering Program, The University of Texas at Austin, Texas, 2012.

[68] M. . T. E. Heinrich, . F. Kelch, . P. Magne and A. Emadi, "Investigation of Regenerative Braking on the Energy Consumption of an Electric Taxiing System for a Single Aisle Midsize Aircraft," IEEE, McMaster University, Hamilton, ON, Canada, 2014.

[69] M. Krosche and W. Heinze, "A Robustness Analysis of a Preliminary Design of a CESTOL Aircraft," Institute of Scientific Computing Technische Universität Braunschweig, Braunschweig, Germany, 2014.

[70] C. Werner-Spatz, W. Heinze , P. Horst and R. Radespiel, "Multidisciplinary conceptual design for aircraft with circulation control high-lift systems," Deutsches Zentrum für Luft- und Raumfahrt, 2012.

[71] H. Schlichting and E. Truckenbrodt, Aerodynamik des Flugzeuges, Berlin, Heidelberg : Springer-Verlag , 1969.

[72] D. Howe, Aircraft Conceptual Design Synthesis, London and Bury St Edmunds, UK : Professional Engineering Publishing Limited, 2000 .

[73] J. J. Berton, W. J. Haller, P. F. Senick, S. M. Jones and J. A. Seidel , "A comparative propulsion system analysis for the high-speed civil transport," Nasa, Glenn Research Center, Cleveland, Ohio, 1995.

[74] S. ZhiQiang, C. ShiChun, W. Zhe and H. PeiLin, "High mixing effectiveness lobed nozzles and mixing mechanisms," School of Aeronautic Science and Engineering, Beijing University of Aeronautics and Astronautics, Beijing, China , 2015.

[75] Special Course on Fundamentals of Fighter Aircraft Design, Advisory Group for Aerospace Research and Development, North Atlantic Treaty Organization, 1987.

[76] H. G. Münzberg, Flugantriebe, Grundlagen, Systematik und Technik der Luft- und Raumfahrtantriebe, Berlin Heidelberg : Springer-Verlag , 1972.

[77] W. J. Bräunling, Flugzeugtriebwerke, Grundlagen,Aero-Thermodynamik,ideale undrealeKreisprozesse,Thermische Turbomaschinen,Komponenten, EmissionenundSysteme, 4 ed., Berlin Heidelberg: SpringerVieweg, 2015.

[78] F. Schmidt and S. Staudacher, "Generalized Thermodynamic Assessment of Concepts for Increasing the Efficiency of Civil Aircraft Propulsion Systems," ASME Turbo Expo 2015: Turbine Technical Conference and Exposition, Montreal, Quebec, Canada, 2015.

[79] H. Rick, Gasturbinen und Flugantriebe, Berlin, Heidelberg: Springer Vieweg, 2013.

[80] General Electric Company , "GE REPORTS," 2017. [Online]. Available: http://www.gereports.com/space-age-cmcs-aviations-new-cup-of-tea/. [Accessed 07 June 2017].

[81] A. Urlaub, Flugtriebwerke, Grundlagen, Systeme, Komponenten, Berlin Heidelberg : Springer-Verlag , 1991.

[82] J. D. Anderson, Jr., Modern Compressible Flow, 2 ed., ew York St Louis San Francisco Auckland Bogota Caracas Hamburg Lisbon London Madrid Mexico Milan Montreal New Delhi Oklahoma City Paris San Juan Sao Paulo Singapore Sydney Tokyo Toronto: McGraw-Hill Publishing Company, 1990.

[83] K. Rypdal , "Aircraft Emissions," Good Practice Guidance and Uncertainty Management in National Greenhouse Gas Inventories, Norway, 1995.

[84] M. Gauss, I. S. A. Isaksen, D. S. Lee and O. A. Søvde, "Impact of aircraft NOx emissions on the atmosphere – tradeoffs to reduce the impac," Atmospheric Chemistry and Physics, 2006.

[85] J. Faber , D. Greenwood , D. Lee , M. Mann , P. Mendes de Leon , D. Nelissen , B. Owen , M. Ralph , J. Tilston , A. van Velzen and G. van de Vreede , "Lower NOx at Higher Altitudes Policies to Reduce the Climate Impact of Aviation NOx Emission," CE Delft Solutions for environment, economy and technology, 2008.

[86] S. C. Olsen, D. J. Wuebbles and B. Owen, "Comparison of global 3-D aviation emissions datasets," Atmospheric Chemistry and Physics, 2013.

[87] A. H. Lefebvre and D. R. Ballal, GAS Turbine Combustion, Alternative Fuels and Emissions, 3 ed., Florida, USA: Taylor and Francis Group, 2010.

[88] M. Aigner and U. Riedel, "Einführung in die Verbrennung, Skript," Institut für Verbrennungstechnik, Universität Stuttgart, 2015.

[89] Committee of Aeronautical Technologies, Aeronautics and Space Engineering Board, Commission on Engineering and Technical Systems, National Research Council, "Aeronautical Technology for the Twenty-First Century," National Academy Press, Washington, D.C. , 1992.

[90] Copyright © , "GasTurb 12, Design and Off-Design Performance of Gas Turbines," GasTurb GmbH, Aachen, Gemany, 2015.

[91] D. N. Anderson, "Effects of Equivalence Ratio and Dwell Time on Exhaust Emissions from an Experimental Premixing Prevaporizing Burner," ASME Paper 75-GT-69, 1975.

[92] G. Leonard and J. Stegmaier, "Development of an Aeroderivative Gas Turbine Dry Low Emissions Combustion System," Journal of Engineering for Gas Turbines and Power, Vol. 116, 1993.

[93] A. Imamura, M. Yoshida, M. Kowano, N. Aruga and N. Yasushi, "Research and Development of a LPP Combustor with Swirling Flow for Low NOx," 37th AIAA/ASME/SAE/ASEE Joint Propulsion Conference & Exhibit, Salt Lake City, Utah, 2001.

[94] Annex 16 to the Convention on International Civil Aviation, Envoronmental Protection, Volume II, Aircraft Engine Emissions, 3 ed., Chicago: International Civil Aviation Organization, 2008.

[95] "edb-emission-databank v23c (web)," 2017. [Online]. Available: https://www.easa.europa.eu/document-library/icao-aircraft-engine-emissions-databank.

[96] R. Radespiel, "Potenziale und Anforderungen des aktiven Hochauftriebs, Foliensatz," Technische Universität Braunschweig, Wissenschaftstag 2010, Institut für Faserverbundleichtbau und Adaptronik, DLR Braunschweig, 2010.

[97] C. Werner-Spatz , W. Heinze , H. Peter and R. Radespiel, "Multidisciplinary conceptual design for aircraft with circulation control high-lift systems," Deutsches Zentrum für Luft- und Raumfahrt, Braunschweig, 2012.

[98] F. Dubs, Aerodynamik der reinen Unterschallströmung, vol. 2, Basel/Stuttgart: Birkhäuser, 1966.

[99] Airbus, "A321neo specs," 2017. [Online]. Available: http://www.aircraft.airbus.com/aircraftfamilies/passengeraircraft/a320family/a321neo/. [Accessed 17 June 2017].

[100] Airbus, "A350-900 specs," 2017. [Online]. Available: http://www.aircraft.airbus.com/aircraftfamilies/passengeraircraft/a350xwbfamily/a350-900/. [Accessed 17 June 2017].

[101] B. Carey, "Honeywell, Safran Demo Electric Taxiing System For Airlines," *AINonline*, 2013.

[102] R. Guo, Y. Zhang and Q. Wang, "Compariso of emerging ground propulsion systems for elctrified aircraft taxi operations," Department of Civil and Environmental Engineering, University of South Florida, Tampa, USA, 2014.

[103] N. Dzikus, J. Fuchte, A. Lau and V. Gollnick, "Potential for Fuel Reduction through Electric Taxiing," 11th AIAA Aviation Technology, Integration, and Operations Conference, 2011.

[104] D. Scholz, "7 Flugzeugsysteme," in *Handbuch der Luftfahrzeugtechnik*, K. W. P. H. Cord-Christian Rossow, Ed., München, Carl Hanser Verlag , 2014, pp. 701-805.

[105] I. Moir and A. Seabridge, Aircraft Systems, Mechanical, electrical, and avionics subsystems integration, 4 ed., The Atrium, Southern Gate, Chichester, West Sussex PO19 8SQ, England : John Wiley & Sons Ltd, 2008.

[106] N. Dickson, "Aircraft Noise Technology and International Noise Standards," set of slides, ICAO Air Transport Bureau, Warsaw, 2015.

[107] EASA – European Aviation Safety Agency , "Jet aeroplanes noise database," 2017. [Online]. Available: URL: https://www.easa.europa.eu/system/files/dfu/MAdB%20JETS%20%28170210%29.xlsx . [Accessed 2017 06 19].

[108] L. H. Fishbach, L. E. Stitt, J. R. Stone and J. B. Whitlow, "NASA Research in Supersonic Propulsion: A Decade of Progress," NASA-TM-82862, 1982.

[109] A. Agarwal and A. P. Dowling, "The calculation of acoustic shielding of engine noise by the silent aircraft airframe," AIAA Paper 2005-2996, 2005 .

[110] M. Li, M. Smith and X. Zhang, "Measurement and control of aircraft's landing gear broadband noise," Aerosp Science Technologz 23, pp. 213-223 , 2012.

[111] M. Pott-Pollenske , " Splitter plate and deceleration plate noise test, report," OPENAIR-DLR-D4.1.6-D4.1.7–R1.0, 2010.

[112] D. You , H. Choi , C. Myung-Ryul and K. Shin-Hyoung , "Control of flow-induced noise behind a circular cylinder using splitter plates," AIAA, 1998.

[113] C. M. Darden, "Sonic Boom Theory: Its Status in Prediction and Minimization," NASA Langley Research Center, Hampton, 1977.

[114] G. B. Whitham, "The Flow Pattern of a Supersonic Projectile," Communications on pure and applied mathematics, vol. v, 301-348, University of Manchester, England, 1952.

[115] H. W. Carlson, "Simplified Sonic-Boom Prediction," NASA, Technical Paper 1122, Langley Research Center, Hampton, Virginia, 1978.

[116] D. N. May, "The Loudness of Sonic Booms heard Outdoors as simple Functions of Overpressure and rise Time," Journal of Sound and Vibration , University of Southampton, Southampton SO9 5NH, England , 1971.

[117] S. S. Stevens, J. Volkmann and E. B. Newman, "A Scale for the Measurement of the Psychological Magnitude Pitch," The Journal of the Acoustical Society of America, Harvard University, Cambridge, Massachusetts and Swarthmore College,S warthmore, Pennsylvani, 1936.

[118] S. S. Stevens, "Perceived Level of Noise by Mark VII and Decibels (E)," Acoustical Society of America, Laboratory of Psychophysics, Harvard University, Cambridge, Massachusetts, 1971.

[119] D. J. Maglieri and K. J. Plotkin, Aeroacoustics of Flight -Vehicles: Theory and- Practice, Chapter 10. Sonic Boom, vol. 1, Hampton, Virginia: Harvey H. Hubbard NASA Langley Research Center, 1991.

[120] P. A. Henne , D. C. Howe, R. R. Wolz and J. L. Hancock, "Supersonic Aircraft with Spike for Controlling and reducing Sonic Boom". United States Patent US 8,789,789 B2 , 29 July 2014.

[121] L. Lindsay and D. J. Maglieri, "Ground Measurements of Airplane Shock Wave Noise for Mach Numbers to 2.0 and Altitudes to 60,000 Ft," National Aeronautics and Space Administration, Langley Research Center, Langley Field, Va., 1960.

[122] M. Dutta, K. Patten and D. Wuebbles, "Parametric analyses of potential effects on stratospheric and tropospheric ozone chemistry by a fleet of supersonic business jets projected in 2020 atm.," NASA, Glenn Research center, 2004.

[123] M. Bagshaw, "Cosmic radiation in commercial aviation," Travel medicine and infectious disease, 2008.

[124] F. S. Preston , "Eight years' experience of Concorde operations: medical aspects," Journal ofthe Royal Society ofMedicine, Volume 78 , 1985.

[125] R. W. Hess and H. P. Romanoff, "Aircraft Airframe Cost Estimating Relationships," Rand Corp., Rept. R3255-AF, Santa Monica, CA, 1987.

[126] J. L. Birkler, J. B. Garfinkle and K. E. Marks, "Development and Produc tion Cost Estimating Relationships for Aircraft Turbine Engines," Rand Corp., Rept. N-1882-AF, Santa Monica, CA, 1982.

[127] S. Borderick, "Boom Order Book Up To 76," 2017. [Online]. Available: :https://www.ainonline.com/aviation-news/airtransport/2017-06-20/boom-order-book-76-ceo-says. [Accessed 2017 20 June].

[128] B. Chudoba, G. Coleman, K. Roberts, B. Mixon, B. Mixon and A. Oza, "What Price Supersonic Speed? – A Design Anatomy of Supersonic Transportation – Part 1," 45th AIAA Aerospace Sciences Meeting and Exhibit, Reno, Nevada , 2007.

[129] F. George, "Aviation Week," 2014. [Online]. Available: http://aviationweek.com/business-aviation/gulfstream-announces-g650er. [Accessed 24 June 2017].

[130] K. Matsushima, K. Kusunose, D. Maruyama and T. Matsuzawa, "Numerical Design and Assessment of a Biplane as Future Supersonic Transport - Revisiting Busemanns's Biplane," 25th International Congress of the Aeronautical Science, 2006.

[131] S. Hollmeier , "Betriebswirtschaftliche Aspekte der Luftfahrtindustrie," Deutsche Lufthansa AG, Institut für Luftfahrtantriebe Universität Stuttgart, Stuttgart, 2015.

[132] J. Roeder, Giganten am Himmel, Großflugzeuge 1910 - heute, München: Rudolf Leuthold Verlag, 1982.

[133] Fightglobal, "Engine deadline slips, but Aerion nears selection," *Flight International* , no. 8 - 14 November, p. 15, 2016.

[134] Boom Technology, Inc, "Boom," 2017. [Online]. Available: https://boomsupersonic.com/. [Accessed 19 June 2017].

[135] Spike Aerospace, Inc., "Spike Aerospace," 2017. [Online]. Available: http://www.spikeaerospace.com/. [Accessed 19 June 2017].

[136] H. Smith , "A review of supersonic business jet design Issues," The Aerospace Journal, Paper No. 3207, Cranfield, UK, 2007.

[137] Wikipedia, "Tupolew Tu-444," 2017 . [Online]. Available: https://de.wikipedia.org/wiki/Tupolew_Tu-444. [Accessed 19 June 2017].

[138] QSST, [Online]. Available: http://sai-qsstx.com/index.html. [Accessed 19 June 2017].

[139] Wikipedia, "SAI Quiet Supersonic Transport," [Online]. Available: https://de.wikipedia.org/wiki/SAI_Quiet_Supersonic_Transport. [Accessed 19 June 2017].

[140] K. P. Shepherd and B. M. Sullivan, "A Loudness Calculation Procedure Applied to Shaped Sonic Booms," NASA Technical Paper 3134, Hampton, Virginia, 1991.

[141] R. D. Johnson and W. D. Robinson, "Procedure for Calculating the Loudness of Sonic Bangs," Acustica, vol. 21. no. 6, 1969.

[142] I. H. Abbott and A. E. von Doenhoff, Theory of Wing Section, New York: Dover Publications, 1959.

[143] S. F. Hoerner, Fluid-Dynamic Drag, Bakersfield: Liselotte A. Hoerner, 1965.

[144] C. Perkins and R. Hage, Airplane Performance, Stability, and Control, New York: Wiley, 1949.

[145] J. Roskam and C.-T. E. Lan , Airplane Aerodynamics and Performance, Kansas: Design, Analysis and Research Corporation , 1997.

[146] J. Roskam, Part III, Layout design of cockpit, fuselage, wing and empenage: Cutaways and inboard profiles, Ottawa, Kansas: Roskam Aviation and Engineering Corporation, 1986.

[147] D. Scholz, Skript zur Vorlesung Flugzeugentwurf, Hamburg: Fachhochschule Hamburg , 1999.

[148] K. Wolf, P. Horst and C. C. Rossow, Handbuch der Luftfahrzeugtechnik, München: Hanser, 2014.

[149] "HIgh Speed AirCraft (HISAC), A European`` Integrated Project'', Slides," Vienna, 2006.

[150] M. Yonezawa, H. Yamashita, S. Obayashi and K. Kusunose, "Investigation of Supersonic Wing Shape Using Busemann Biplane Airfoil," 45th AIAA Aerospace Sciences Meeting and Exhibit , Reno, Nevada, 2007.

[151] Honeywell and Safran/Messier-Bugatti-Dowty , "Set of slides, Electric green taxiing system," Presentation to Arts et Métiers, 2013.

[152] D. Schmidt, Luftfahrttechnik, Flugzeugentwurf, Skript zur Vorlesung, München: Technische Universität München, Lehrstuhl für Luftfahrttechnik, 1998.

Appendix

A. Nomenclature

A''	Second derivative of the equivalent body area due to volume with respect to x
C_D	Drag coefficient
C_L	Lift coefficient
c_{TL}	Thrust specific fuel consumption
D	Aerodynamic Drag
l'	First derivation with respect to x of the net force normal to the stream direction inclined by θ
L	Aerodynamic Lift
L^*	Length of equivalent body
$m_{landing}$	Landing mass
m_{start}	Start mass
n	Number of flat plate airfoils
q	Dynamic pressure
R	Range
s_{AS}	Acceleration-stop distance
s_{TO}	Take-off distance
s_{TOEF}	Take-off engine failure distance
s_{TOFL}	Take-off field length
t	Time
v	Velocity
v_j	Jet velocity
v_0	Aircraft speed
x	Longitudinal coordinate
x, y, z	Cartesian coordinates
x_1, x_2	Dummy variables

α	Angle of attack
α_s	Angle of attack for n flat plate airfoils
β	Equals $\sqrt{Ma^2 - 1}$
$\eta_{propulsion}$	Propulsive efficiency
η_{th}	Thermal efficiency
θ	Angle between the negative z-axis and the line of intersection of the Mach plane with the y-z plane
κ	Heat capacity ratio
μ	Mach angle $\sin^{-1}(1/Ma_\infty)$
π_c	Compressor pressure ratio
τ_0	Total pressure ratio due to the ram effect

B. List of Abbreviations

AC	Aerodynamic Center
APU	Auxiliary Power Unit
BPR	Bypass-ratio
CFD	Computational Fluid Dynamics
CG	Center of Gravity
CMC	Ceramic Matrix Composites
CO	Carbon Monoxide
CS-25	Certification Specification for Large Airplanes
DLR	German Aerospace Center
EGTS	Electrical Ground Taxi System
EHA	Electro-Hydrostatic Actuator
EI	Emission Index
EMA	Electro-Mechanical Actuators
EPNdB	Effective Perceived Noise Level
FAR	Federal Aviation Regulations
FBW	Fly-By-Wire
HELESA	High Efficient Low Emission Supersonic Aircraft
HISAC	Highspeed Aircraft
IAG	Institute of Aerodynamics and Gas dynamics of the University of Stuttgart
ICAC	Initial climb altitude capability
ICAO	International Civil Aviation Organization
ISA	International Standard Atmosphere
JAXA	Japan Aerospace Exploration Agency
L/D	Lift-to-drag ratio
LPP	Lean Premix Prevaporized
LTO	Landing and Take-off
LuftVO	Luftverkehrs-Ordnung
MAC	Mean Aerodynamic Chord
MEA	More Electric Aircraft
mSv	Millisievert
Ma	Mach number
MTOM	Maximum Take-off Mass
NASA	National Aeronautics and Space Administration
NEXST-1	National Experimental Supersonic Transport Project
NOx	Nitrogen Oxide
OEI	One Engine Inoperative
OLED	Organic Light-Emitting Diode
OME	Operating Mass Empty
PLdB	Perceived Noise Level
SiC-SiC	Silicon-Carbide Fiber reinforced Silicon-Carbide Ceramics
SL	Sea Level
TOFL	Take-off Field Length
UHC	Unburned Hydrocarbons

C. List of Figures

Figure 1. Time saving potential [1] 1
Figure 2. Structural design with cut-outs of the subsonic and supersonic wing position 2
Figure 3. Schematic design process 3
Figure 4. Design diagram 3
Figure 5. Smallest and biggest cross-section 4
Figure 6. Cabin layout 4
Figure 7. Cabin side view 5
Figure 8. Influence of flap deflection on the lift-to-drag ratio 5
Figure 9. Thrust and drag against Mach number and altitude 6
Figure 10. Lift to drag ratio against the Mach number 6
Figure 11. Drag Coefficients at supersonic, transonic and subsonic/transonic Cruise 7
Figure 12. Drag polar for different mission segments 7
Figure 13. Equivalent bodies for the angle θ of 0° 8
Figure 14. Equivalent bodies for the angle θ of 135° 8
Figure 15. Supersonic laminar flow wing by Tracy [18] 10
Figure 16. Busemann bi-plane [143] 10
Figure 17. Geometries of the tail-plane design study 12
Figure 18. Fuselage length versus MTOM and fuselage weight 13
Figure 19. Optimization of the fuselage length 13
Figure 20. Lifting shock wave cancellation module [56] 13
Figure 21. Aerodynamic center and center of gravity for variable forward- and backward swept wings 15
Figure 22. Thrust dependence from Mach-number and BPR 16
Figure 23. The intake 17
Figure 24. NOx emission index for different flight segments 18
Figure 25. Landing gear mechanism 19
Figure 26. Landing gear position 19
Figure 27. EGTS [151] 19
Figure 28. Possible maximum range for different cruising speeds 21
Figure 29. Far-field pressure signatures for different mission segments 21
Figure 30. Payload-Range diagram 21
Figure 31. Range and time for different super/trans cruise fractions 22
Figure 32. Range and time for different super/sub cruise fractions 22
Figure 33. Hysteresis effect of a Busemann bi-plane [130] 37
Figure 34. 2D analysis of the Busemann wave rider 37
Figure 35. 3D analysis of the Busemann wave rider 37
Figure 36. Landing and Takeoff drag polar 38
Figure 37. Overturn angle 38
Figure 38. Pressure signature from [93] 39
Figure 39. Payload-range diagram for different cruise Mach numbers 39

D. List of Tables

Table 1. General HELESA data 2
Table 2. Data for different mission segments 5
Table 3. Wing configuration matrix 9
Table 4. Data from the tail-configuration comparison 12
Table 5. Component masses 14
Table 6. Engine data for different segments 17
Table 7. General engine data 15
Table 8. take-off distances 18
Table 9. Maximum pressure differences, duration of pressure disturbance, the rise time of the first pressure peak and the loudness level for different mission segments 20
Table 10. Noise levels of the HELESA design and comparable aircraft at airport reference points. 20
Table 11. Ranges for different Mach numbers and payload 22
Table 12. Low sonic boom technologie 38
Table 13. Aircraft costs 40
Table 14. Data from other supersonic Aircraft Designs 41

E. Three side View

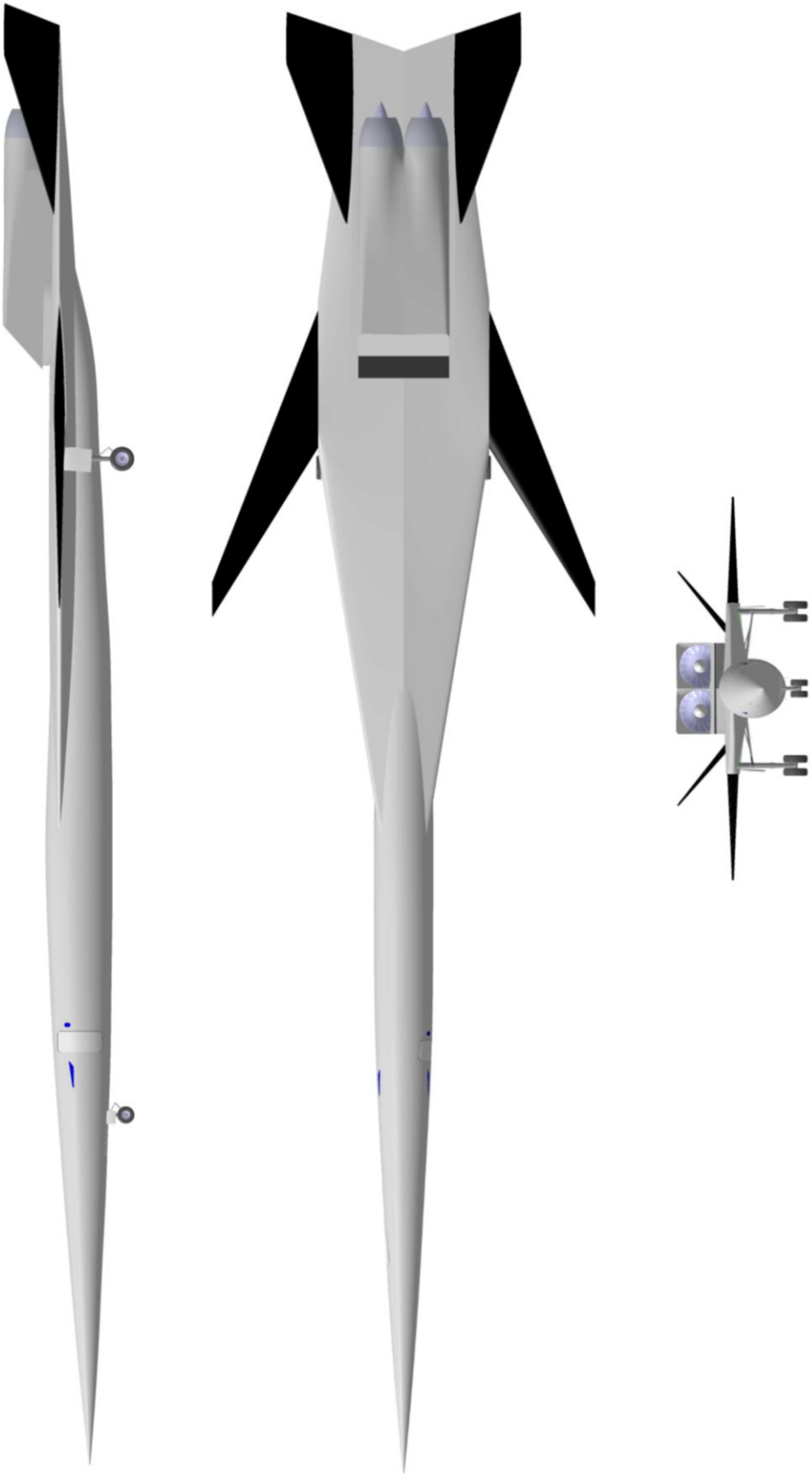

F. List of postal addresses of the students

Schaupp	Dominik	Traubenstrasse 53, 70176 Stuttgart, Germany
Silberhorn	Daniel	Effeltricher Strasse 51, 90411 Nürnberg, Germany

G. List of Authors

Chapter	***Author (text & content)***
1 Introduction	Silberhorn
2 The Configuration	Silberhorn
3 Design Process	Silberhorn
4 The HELESA Design	
4.1 Cabin Design	Silberhorn, Schaupp
4.2 Aerodynamics	
4.2.1 Subsonic Regime	Silberhorn
4.2.2 Transonic Regime	Silberhorn
4.2.3 Supersonic Regime	Silberhorn
4.2.4 The Wing	Silberhorn
4.2.5 Canard versus V-Tail	Silberhorn
4.2.6 Aerodynamic Efficiency versus structural Mass	Silberhorn
4.2.7 Wave Rider	Schaupp
4.3 Mass Prediction and Stability	Silberhorn
4.4 Propulsion	Silberhorn
4.5 Systems	Silberhorn
4.6 Noise	
4.6.1 ICAO Cycle	Schaupp
4.6.2 Sonic Boom	Silberhorn
4.7 The Mission	Silberhorn
4.8 Concluding Studies	Silberhorn, Schaupp
5 Conclusion	Silberhorn

H. Hysteresis effect for a supersonic Biplane

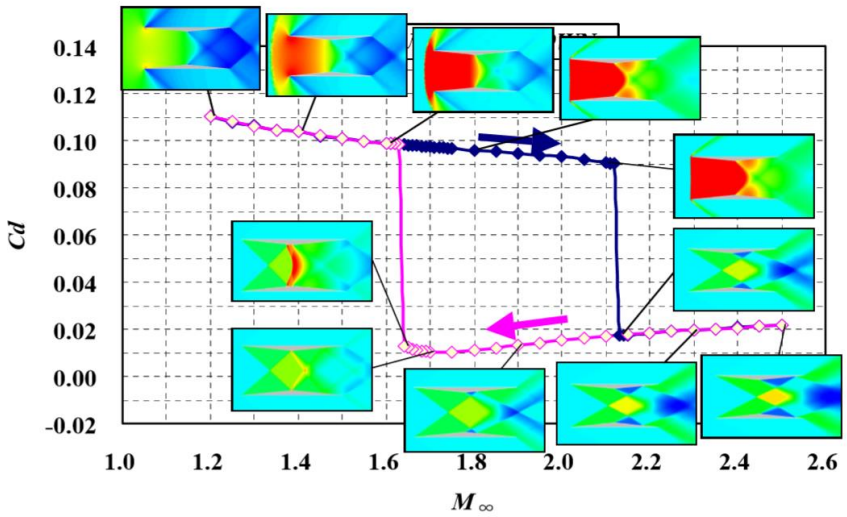

Figure 34. Hysteresis effect of a Busemann bi-plane [130]

I. Busemann Wave Rider

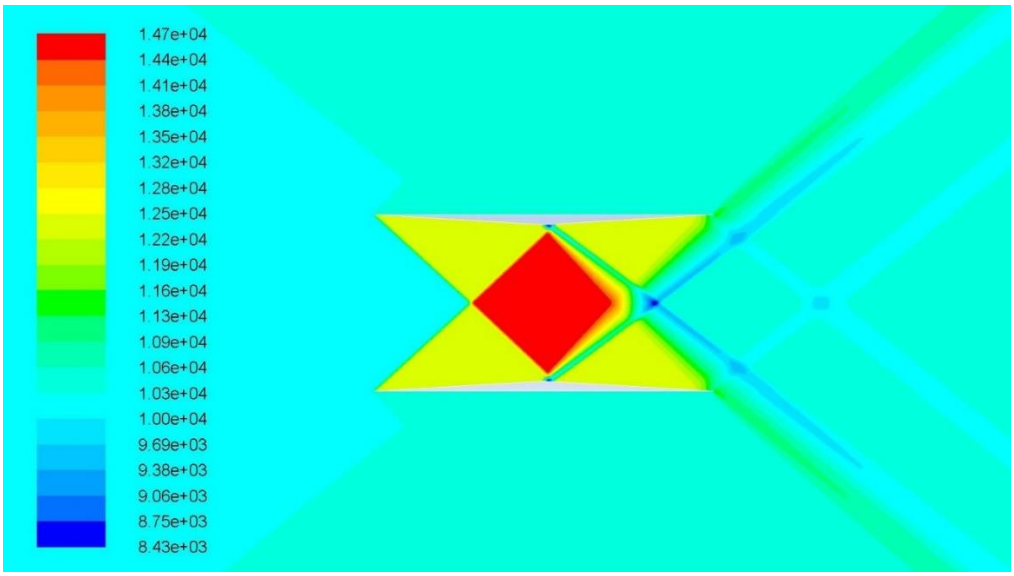

Figure 35. 2D analysis of the Busemann wave rider

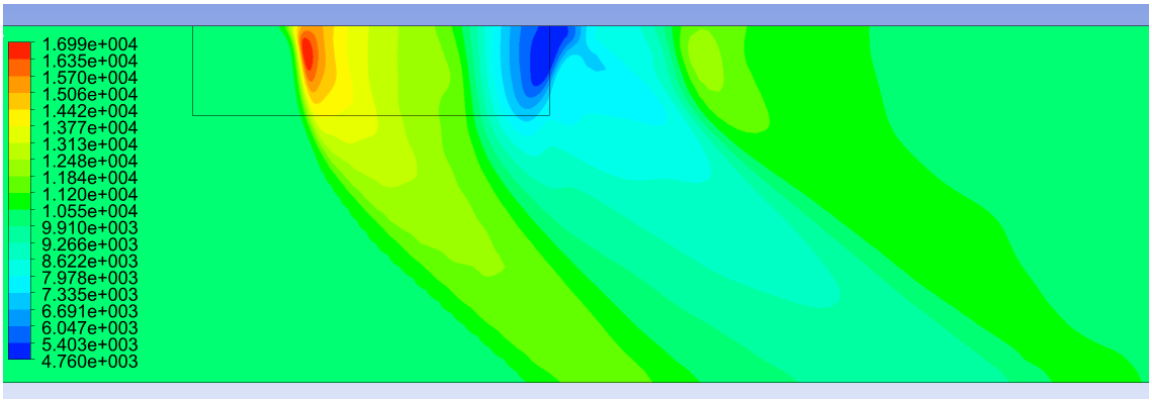

Figure 36. 3D analysis of the Busemann wave rider

J. Landing and Takeoff drag Polar

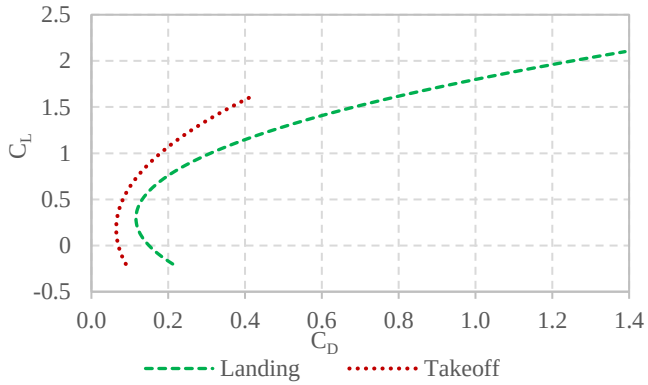

Figure 37. Landing and Takeoff drag polar

K. Low Sonic-Boom Techniques

Low Boom adaption	Feasibility	Effect on Efficiency	Effect on Boom
Special Nose Shaping	++	-	+
Front Spike	++	-	+
Rear Spike	++	-	**0 (+)**
Greater slenderness ratio	**0**	--	+
Blunt nose	++	---	++
Greater effective slenderness ratio with exhaust jet	+	**0**	**0 (+)**
Wing dihedral	++	--	++
Thermal fin	-	---	+
Reflection plate	++	---	++
Flight-formation	**0**	**0**	**+ (0)**
Greater effective slenderness ratio with Laser-beam	---	**0**	+
Microwaves, Explosive etc.	---	-	**+?**

Table 12. Low sonic boom technologie

L. Landing gear Position

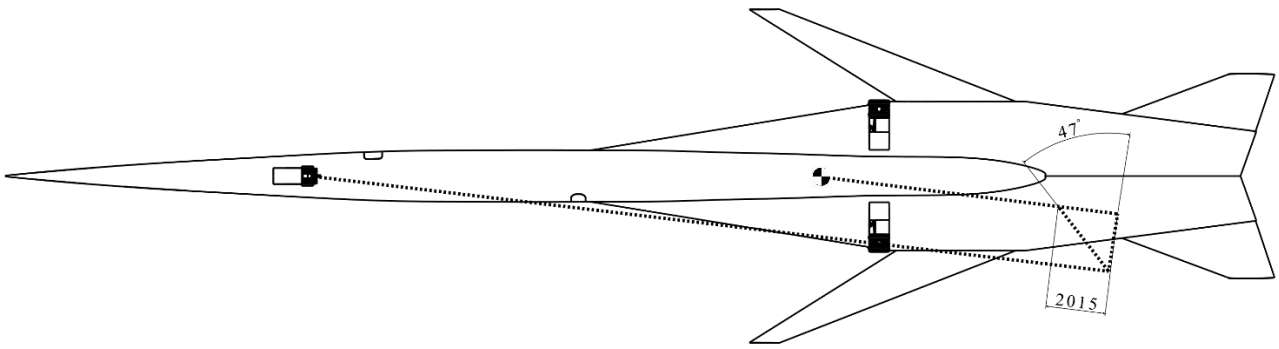

Figure 38. Overturn angle

M. Sonic Boom Pattern

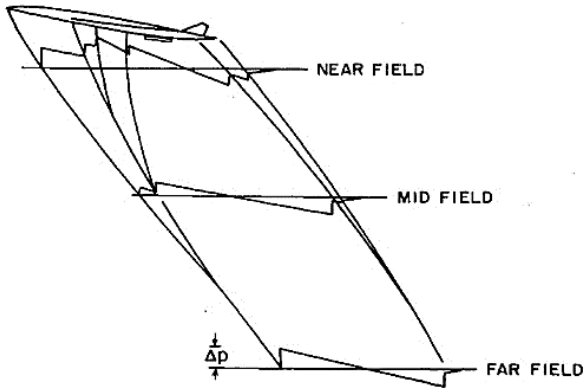

Figure 39. Pressure signature from [93]

N. Payload-Range Diagram for different Mach numbers

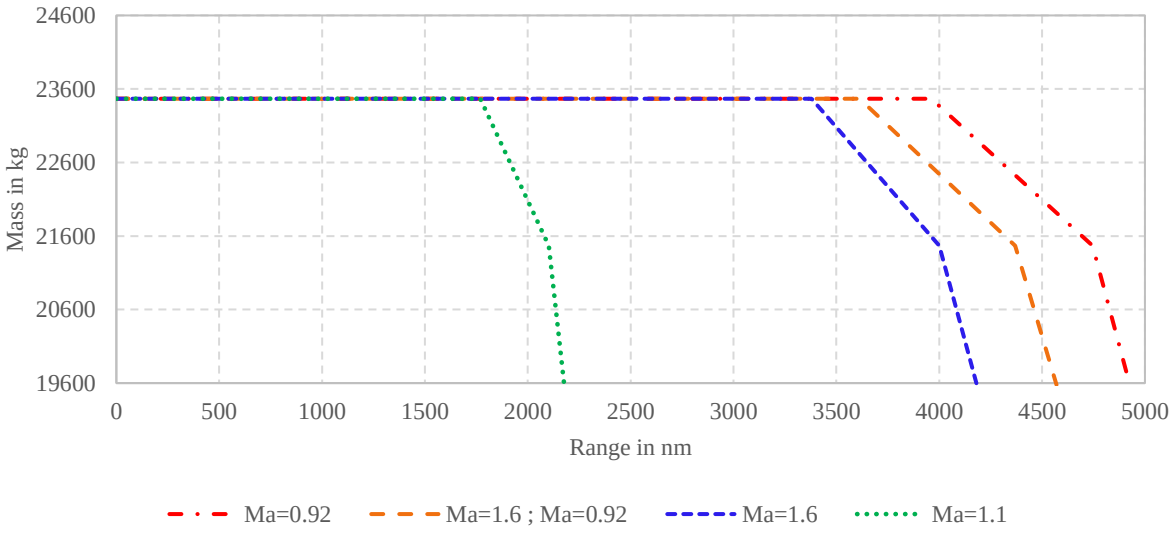

Figure 40. Payload-range diagram for different cruise Mach numbers

O. Aircraft Costs

		Cost/Aircraft [$]
RDT&E and production		
	Engineering	21,062,369
	Tooling	10,947,641
	Manufacturing	23,826,530
	Quality control	3,492,288
	Development support	5,391,521
	Flight test	1,169,216
	Manufacturing materials	12,365,041
	Engine	14,528,807
	Avionics	10,241,133
	Interior	180,000
	Initial spare (+10%)	10,320,455
	Fudge factor* (-5,5%)	-5,937,357
	Total cost	107,587,648
Operation costs per flight		
	Fuel	28,800
	Maintenance	5,921
	Crew	4,014
	Insurance	774
	Depreciation [131]	3,442
	Traffic control [131]	2,458
	Airport charges [131]	3,934
	Total	49,177

* Fudge factor contains overprediction of the DAPCA IV Model and adjustments due to inflation, [9]

Table 13. Aircraft costs

P. Visualization of Missions

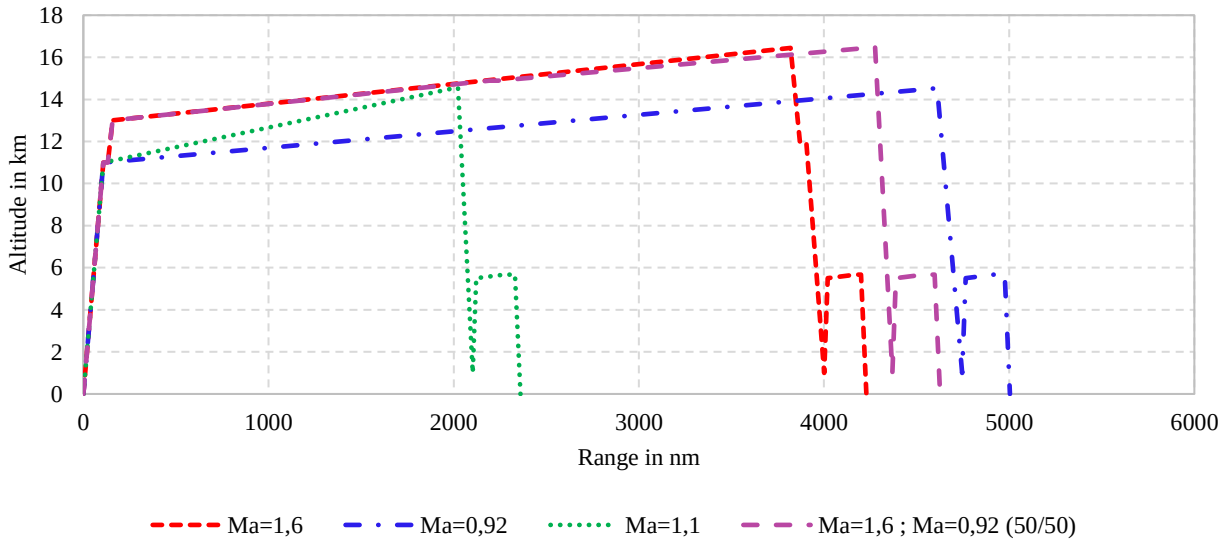

Q. Table with data of other supersonic designs and aircraft

	MTOM [kg]	Design Range [nm]	Cruise Speed [Ma]	Capacity [-]	Ref. Wing Area [m^2]	Take-off Thrust [kN]
Aérospaciale - BAC Concorde	185,065 [132]	3,552.9* [132]	2.02 [124]	128 – 144 [132]	358.3 [132]	4x137.3(dry) 4x169.3(wet) [132]
Tupolew Tu-144	180,000 [132]	3,510** [132]	2.3 [132]	100 – 140 [132]	438 [132]	4x169.1(wet) [132]
Aerion AS2	54,884 [24]	4,750 [24]	1.4 [24]	8 – 10 [12]	125 [24]	3 x 71.2-75.6 [133]
Boom		4,500*** [134]	2.2 [134]	55 [134]		
Spike S-512	52,163 [135]	5,580 [135]	1.6 [135]	Max. 18 [135]	104,5 [135]	2 x 88.9 [135]
Sukhoi-Gulfstream S-21	51,800 [12]	2,715 [12]	1.4 [12]	6 – 10 [12]		220.6 [12]
Tupolev Tu-444	41,005 [136]	4,660 [136]	2 [136]	6 – 10 [136]	136 [137]	190.3 [137]
NASA X-plane	10,200 [12]		1.42 [12]	1 [12]		60.0 [12]
SAI Quiet Supersonic Transport	69,400 [12]	4,000 [12]	1.6 [138]	12 – 16 [139]		294.0 [12]
JAXA SSBJ-M	36,000 [12]	3,500 [12]	1.6 [12]	10 [12]		140.0 [12]
Gulfstream Aerospace QSJ	45,400 [12]	4,800 [12]	1.8 [12]	6 – 10 [12]		294.0 [1]
Uni Stanford	43,100	4,000	1.6	6 - 8		
HISAC-A (Dassault)	51,100	4,000	1.6	8		220.0
HISAC-B1 (Alenia)	60,500	5,000	1.6	8		313.5
HISAC-C (Sukhoi)	53,300	4,000	1.8	8		292.6

Table 14. Data from other supersonic Aircraft Designs

* *Max. payload without reserve fuel*

** *Max. payload without reserve fuel at Mach 1.9*

*** *Routes over 4,500nmi include a brief tech stop*

R. Structural Design I

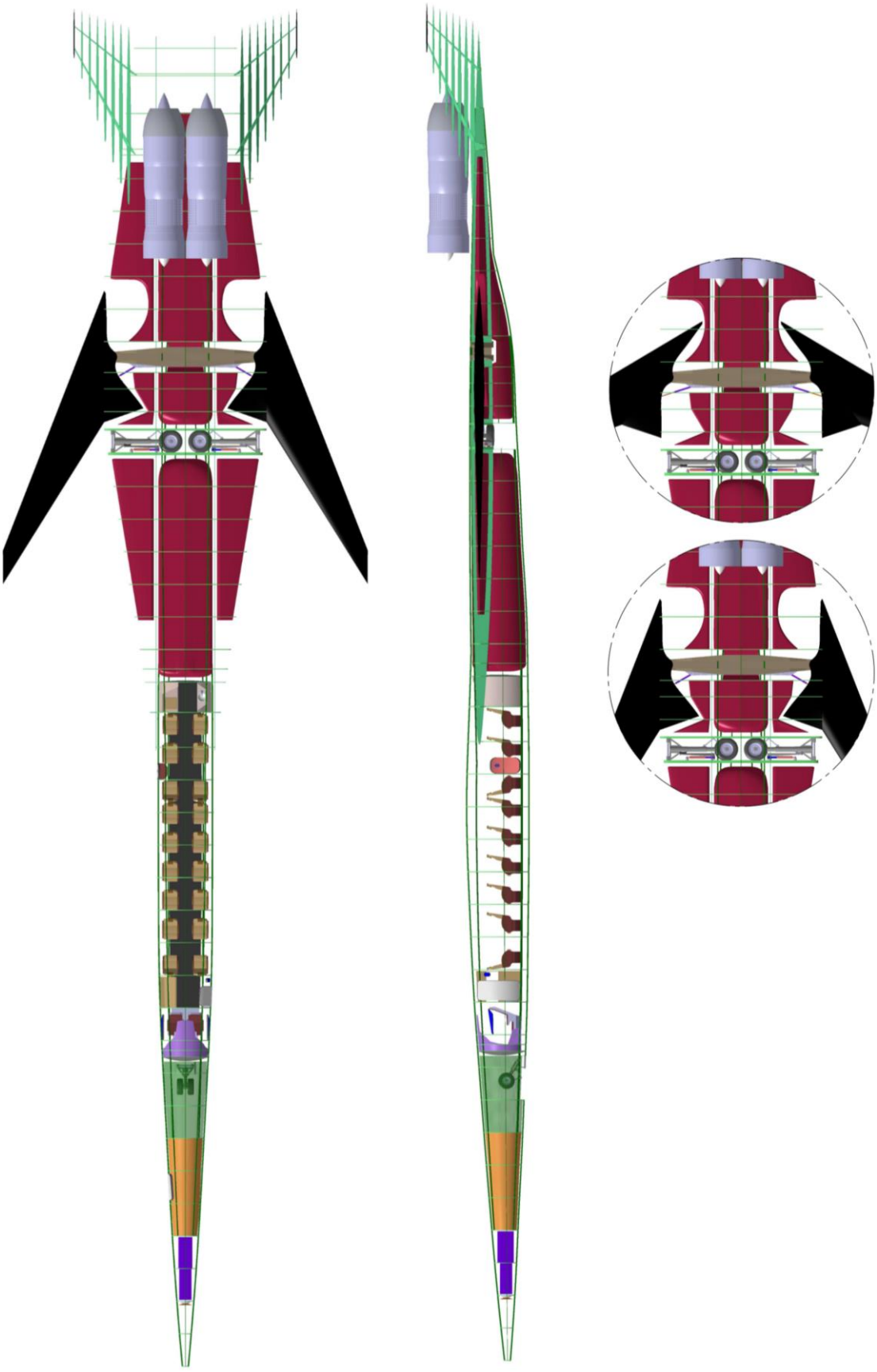

S. Structural Design II

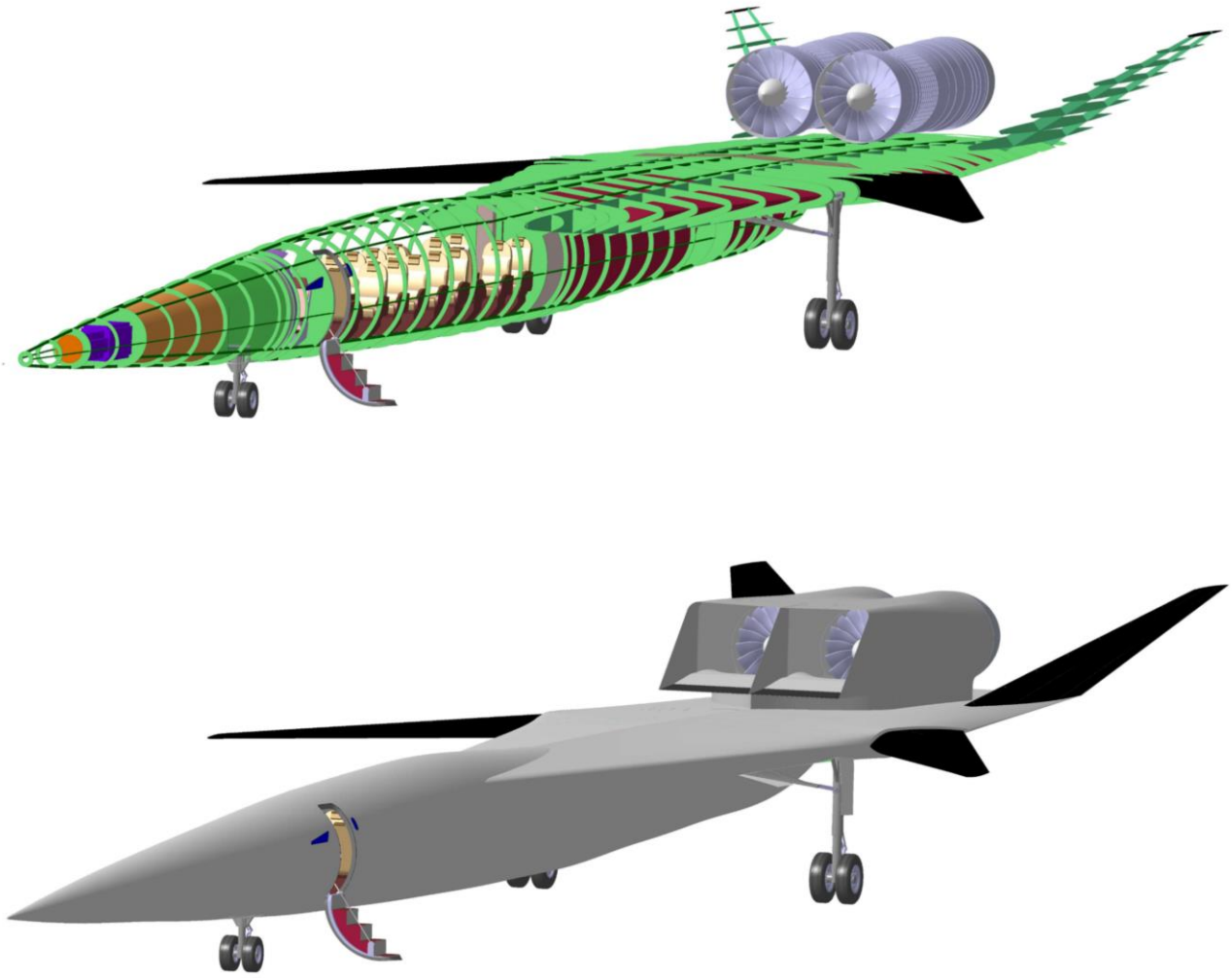

T. Aircraft Pictures